Materials & Design 241 (2024) 112973

Contents lists available at ScienceDirect

Materials & Design

journal homepage: www.elsevier.com/locate/matdes

Remnant polarization and structural arrangement in P(VDF-TrFE) electrospun fiber meshes affect osteogenic differentiation of human mesenchymal stromal cells

Bahareh Azimi [a], Massimiliano Labardi [b], Mohammad Sajad Sorayani Bafqi [a,c], Teresa Macchi [d], Claudio Ricci [a], Veronica Carnicelli [e], Lorenzo Scarpelli [a,b], Istiak Hussain [f], Francesca Matino [g], Michelangelo Scaglione [d], Dario Pisignano [g,h], Andrea Lazzeri [a], Mohammed Jasim Uddin [f], Luana Persano [g], Serena Danti [a,b,*]

[a] Department of Civil and Industrial Engineering, University of Pisa, Pisa, Italy
[b] Institute for Chemical-Physical Processes, National Research Council (CNR-IPCF), Pisa, Italy
[c] Department of Textile Engineering, Amirkabir University of Technology (Tehran Polytechnic), Tehran, Iran
[d] Department of Translational Researches and New Technologies in Medicine and Surgery, University of Pisa, Pisa, Italy
[e] Department of Surgical, Medical, Molecular Pathology and Emergency Medicine, University of Pisa, Pisa, Italy
[f] Department of Chemistry, Photonics and Energy Research Laboratory (PERL), University of Texas Rio Grande Valley, Edinburg, TX, USA
[g] NEST, Istituto Nanoscienze-CNR and Scuola Normale Superiore, Pisa, Italy
[h] Department of Physics, University of Pisa, Pisa, Italy

ARTICLE INFO

Keywords:
Piezoelectric
Electrospinning
Tissue engineering
Mesenchymal stem cells
Osteogenesis
Fiber orientation

ABSTRACT

Many tissues and cells are influenced by mechano-electric stimulation, thus the application of piezoelectric materials has recently received considerable attention in tissue engineering. This report investigated electrospun fiber meshes based on poly(vinylidenefluoride-*co*-trifluoroethylene) [P(VDF-TrFE)] as instructive biomaterials for osteogenic differentiation of human mesenchymal stromal cells (hMSCs). The influence played by methyl ethyl ketone (MEK), used as a solvent in place of dimethylformamide (DMF)/acetone mixture, and the effect of rotating velocity of the electrospinning collector on fiber morphology, mechanical and piezoelectric properties were studied. The solvent had noticeable effects on morphology and piezoelectric properties of electrospun fibers, with MEK outperforming DMF/acetone. By increasing the collector velocity up to 4000 rpm, the fiber diameter reduced and the mutual alignment of the fibers increased, corresponding to enhanced mechanical properties and piezo-active β-phase content. However, as a consequence of the diverse mechanical properties of random and aligned fibrous architectures, which ultimately affected the piezoelectric properties, randomly-oriented fibers exhibited higher remnant piezoelectric properties (V_{out} and d_{31} piezoelectric coefficient) than aligned ones. On these scaffolds, hMSCs showed an excellent capability of early osteogenic differentiation, leading to high calcium production. Fiber surface topology, fiber mesh morphology and remnant piezoelectric properties played a determinant role on hMSC osteogenic commitment.

1. Introduction

Tissue engineering presents a brilliant approach to restore faulty organs and tissues which cannot self-regenerate by developing biological substitutes [1]. Scaffolds are critically important components for tissue engineering, as they play a relevant role in tissue growth and

Abbreviations: $\%AB_{red}$, alamarBlue® reduction percentage; AFM, atomic force microscopy; ALP, alkaline phosphatase; d_{31}, piezoelectric coefficient; DAPI, 4′,6-diamidino-2-phenylindole; DMA, Dynamic mechanical analysis; DMF, dimethylformamide; DSC, Differential scanning calorimetry; ECM, extracellular matrix; FBS, fetal bovine serum; FTIR, Fourier Transform Infrared; hMSCs, human mesenchymal stromal cells; MEK, methyl ethyl ketone; P(VDF-TrFE), Poly(vinylidenefluoride-co-trifluoroethylene); PBS, Phosphate Buffered Saline; PVDF, Polyvinylidene fluoride; RH, relative humidity; RT, room temperature; SEM, scanning electron microscopy; Tc, Curie temperature; Tm, melting temperature; $V_{out,\ RMS}$, vibration amplitude output; XRD, X-ray diffraction.

* Corresponding author at: Department of Civil and Industrial Engineering, University of Pisa, Pisa, Italy.
E-mail address: serena.danti@unipi.it (S. Danti).

https://doi.org/10.1016/j.matdes.2024.112973
Received 19 December 2023; Received in revised form 10 March 2024; Accepted 20 April 2024
Available online 22 April 2024

regeneration across a three dimensional (3D) space [2]. Together with 3D architecture and mechanics, (bio)electricity is another important feature of a number of body tissues: among others, bone [3], muscles and inner ear sensory organs [4], remarkably show a sort of piezoelectric behavior, wherein an electrical charge can be ultimately induced or activated by a mechanical stress. Bone is a piezoelectric tissue with piezoelectric constants similar to those of quartz, primarily by virtue of collagen type I, the main component of the organic extracellular matrix (ECM) [5]. For these reasons, it is proposed that the piezoelectric effect plays an important physiological role in bone growth, remodeling and fracture healing [3]. Indeed, it has been evidenced that when the bone is mechanically stressed, electrical signals are produced, which in turn promote tissue growth and remodeling; however, the underlying biological mechanism is still a subject of investigation. Where the bioelectricity driven by mechanical forces has a pivotal role, the application of piezoelectric materials in tissue engineering is invoked to support tissue function [4,6,7].

Among piezoelectric materials, piezopolymers are highly suitable for tissue engineering, thanks to their biocompatibility, flexibility, processability and good piezoelectric response [8]. Since piezoelectric polymers are potentially able to generate transient surface charges under mechanical deformation, they can provide electrical stimulation to cells and promote tissue formation [9]. Polyvinylidene fluoride (PVDF) and its copolymers, such as PVDF-trifluoro ethylene [P(VDF-TrFE)], are among the best performing piezopolymers. Thanks to the chemical strength of the C-F bond, PVDF-based (co)polymers behave as biostable and bioinert materials also in the human body; as a consequence, they are FDA-approved and can also find application in tissue engineering owing to other distinctive properties, nicely combined with their bioinert character [6]. Piezoelectricity in these compounds originates from oriented molecular dipoles formed by a combination of mechanical deformation and electrical poling of the crystallographic phase β [10]. Indeed, the β-phase, which has fully trans-planar zig-zag conformation, is mostly responsible for the obtained piezoelectric response due to its polar structure with oriented hydrogen and fluoride unit cells along with the carbon backbone. In particular, P(VDF-TrFE) is a multifunctional copolymer of PVDF, in which the β-phase is promoted, and therefore the piezoelectricity, with respect to its homopolymer. Moreover, due to their largely thermoplastic behavior, PVDF and P(VDF-TrFE) can be readily processed into solids, films, textiles, and coatings.

Electrospinning is a straightforward and versatile method for fabricating ultrafine fibers from polymer solutions, able to inherently provide both mechanical stretching and electrical poling for transforming some non-polar α-phase into polar β-phase crystals of VDF-based polymers [11–14]. The abovementioned properties feed the considerable interest of tissue engineers and biomaterials scientists towards biocompatible and piezoelectric electrospun fibers enabling electrical stimulation at the cellular level and ultimately promoting tissue function [5,15]. Indeed, the fibrous structure of electrospun meshes (i.e., fibers with diameter range in the order of tens of nanometers to few microns) can mimic ECM fibers, while their piezoelectric character could be highly advantageous for bone regeneration and stimulation [2].

Although operationally simple, the electrospinning process is based on various working parameters, whose influence on the properties of P(VDF-TrFE) fibers has not been completely unveiled yet. The electrospinning parameters can be broadly related to the following: *(a)* solution (e.g., polymer concentration, type of solvent, viscosity, surface tension, conductivity), *(b)* process (e.g., voltage, flow rate, collector type and velocity, tip-to-collector distance), and *(c)* environment (e.g., humidity, temperature) [16], all concurring to influence the conversion of polymer solutions into fibers. Desired fibers can be produced with controllable diameters, composition and morphology only if such parameters are successfully mastered [17–19].

A number of studies have reported on the fabrication of PVDF and P(VDF-TrFE) fibers via electrospinning under selected conditions for different applications [20–26]. Several works have focused on the fabrication of randomly oriented fibers and subsequent thermo-mechanical treatments, such as hot pressing or annealing, aiming at improving the final piezoelectric properties [27–29]. A few studies have also investigated the effect of electrospinning parameters on these properties in the resulting fibers [11,30,31]; however, an in-depth understanding of this relation is still underway. In particular, the comprehension of the simultaneous effect of solvent type and collector velocity on morphology, mechanical and piezoelectric properties of electrospun P(VDF-TrFE) fiber meshes is still challenging. The used solvent is a key factor contributing to the intrinsic properties of the electrospinning solution [32], which might critically affect fiber formation. Volatility, conductivity, boiling point and dipole moment of the solvent are all important factors for achieving uniform and defect-less polymer filaments [33]. Furthermore, the solvent and the environmental conditions play a crucial role in the fabrication of fibers with internal or surface porosity. On the other hand, collector velocity is relevant in affecting mechanical stretching on the fibers and therefore their size, morphology, alignment and mechanical properties. Accordingly, we hypothesized that such parameters would ultimately affect the piezoelectric outcome, which is strongly dependent on fiber structure and alignment, thus influencing the biological response in bone forming cells.

This study aimed at the fabrication and characterization of optimal P(VDF-TrFE) ultrafine fiber scaffolds for bone tissue engineering. The effect of solvent type and collector velocity on morphology and piezoelectric properties of electrospun fiber meshes were investigated through a number of techniques, encompassing morphological (i.e., scanning electron microscopy, atomic force microscopy, gravimetric porosity), physico-chemical (i.e., Fourier-transform infrared spectroscopy, differential scanning calorimetry, X-ray diffraction), mechanical (i.e., tensile and dynamic mechanical) and piezoelectric (i.e., direct and converse piezoelectric coefficients, output voltage) analyses, the latter via different methods. Therefore, the optimal scaffolds produced as random and aligned fiber meshes were tested *in vitro* with human mesenchymal stromal cells (hMSCs) and the early-stage bone ECM production was evaluated. This research explores the effect of remnant piezoelectricity, namely charged surface of piezoelectric materials in rest conditions, on the osteogenic differentiation of hMSCs, which has not been taken into consideration until now.

The successful mastering of electrospinning parameters for PVDF-based nonwovens would enable the fabrication and industrial upscaling of smart micro/nano-structured piezoelectric materials for cellular stimulation.

2. Materials and methods

2.1. Materials

P(VDF-TrFE) powder (70:30 %mol) was purchased from Piezotech Arkema (Pierre-Benite, France), Methyl ethyl ketone (MEK; code 109708) was bought from Merck (Darmstadt, Germany), Dimethylformamide (DMF; code 444926) was supplied by Actu-all Chemicals (Oss, Netherlands). Glacial acetic acid (code 1.00063), acetone (code 32201), absolute ethanol, low-glucose Dulbecco's Modified Eagle Medium (DMEM), L-glutamine, penicillin/streptomycin, heat-inactivated fetal bovine serum (FBS), gelatin (type B, from bovine skin) and TriReagent were obtained from Sigma-Aldrich (Milan, Italy). Lymphoprep was purchased from GE healthcare (Hatfield, UK). Phosphate Buffered Saline (PBS, 1 ×) was bought from Gibco, Thermo Fisher Scientific (Waltham, MA, USA). Fluconazole was supplied from Fresenius Kabi (Verona, Italy). Osteogenic differentiation medium (hMSC differentiation bulletkit osteogenic) was supplied by Lonza (Basel, Switzerland). AlamarBlue® and 4′,6-diamidino-2-phenylindole (DAPI) were purchased from Thermo Fisher Scientific (Waltham, MA, USA). Neutral buffered formalin was obtained from Bio-Optica (Milan, Italy).

Arsenazo III was supplied by Diagnostic Chemicals, Oxford, CT, USA. iScript cDNA Synthesis Kit and SsoAdvanced Universal SYBR Green Supermix were purchased from Bio-Rad (Hercules, CA, USA).

2.2. Production of electrospun fiber meshes

P(VDF-TrFE) was dissolved in DMF/acetone (1:1 v/v) or MEK at a polymer/solvent concentration of 20 % (w/v) and stirred at 300 revolutions per minute (rpm) for 12 h at room temperature (RT). Each polymer solution was loaded into a 10 mL glass syringe, fitted with a blunt tip stainless steel needle (21G × 3/4″) and placed into a syringe pump (NE-300, New Era Pump Systems, Inc., NY, USA). The ground terminal of high voltage supply (S1600079 Linari High Voltage, Linari Engineering s.r.l., Pisa, Italy) was connected to the metal needle, while the positive terminal was connected to the collector; a 35 kV potential was then applied. A static collector made of a plastic plate covered with an aluminum foil, or a cylindrical collector (diameter 8 cm, Linari Engineering s.r.l.), were placed at a distance of 15 cm from the tip of the needle. The polymer solution was injected from the needle in the presence of the electric field at a constant flow rate of 0.016 mL/min. The production of random-to-aligned electrospun fiber meshes was performed by collecting the polymeric jet on the static or rotating collector with collector velocities of 500 rpm, 2500 rpm and 4000 rpm. All the fabrication steps were performed at RT with relative humidity (RH) of about 46% if not differently specified. The fiber meshes were kept in an oven at 60 °C overnight to remove possible solvent traces.

2.3. Morphological characterization

The morphology of the fiber meshes was evaluated by scanning electron microscopy (SEM) using an FEI FEG-Quanta 450 instrument (Field Electron and Ion Company, Hillsboro, OR, USA). The samples were sputtered with gold (Gold Edwards SP150B, UK) before analysis. Image-J software (version 1.46 r; http://imagej.nih.gov) was used to determine the average diameter of 100 fibers obtained from SEM images. The fiber surface topography was also analyzed with atomic force microscopy (AFM) in tapping mode, using a Veeco Instruments Multimode atomic force microscope equipped with a Nanoscope IIIa controller (Veeco Instruments Inc., NY, USA). Non-contact mode silicon cantilevers were used (BudgetSensors Tap300, 300 kHz nominal resonant frequency, and 40 N·m^{-1} nominal spring constant).

The gravimetric porosity of the scaffolds was estimated as:

$$\text{Porosity}\ (\%) = \left(1 - \frac{\rho_{scaffold}}{\rho_{raw}}\right) \times 100 \tag{1}$$

$$\rho_{\text{scaffold}} = \frac{M}{V} \tag{2}$$

where M is the mass, and V the volume of the fabricated scaffolds, measured with a pycnometer (Duran, Germany), while ρ_{raw} is the density of the unprocessed material.

ImageJ analysis was applied to SEM micrographs ($n = 3$) taken at 40,000 × to evaluate size and size distribution of the nanopores at the fiber surface, by considering the equivalent diameter of a circle of the measured nanopore area. In brief, the micrographs were changed to binary colors representing the fibers in white and the void in black, which allowed pore size in the range of 5–550 nm to be detected ($n = 30$). Therefore, the eccentricity of the nanopores was evaluated as follows:

$$e = \frac{\sqrt{(a^2 - b^2)}}{a} \tag{3}$$

Where a and b are the semi-major and semi-minor axis of the ellipes, respectively, and e is the eccentricity. The effect of DMF/acetone on fiber morphology is detailed in Supplementary Note 1.

2.4. Crystalline phase evaluation

The relative fraction of β-phase, $F(\beta)$, was determined by FTIR spectroscopy. The FTIR spectra of electrospun fibers were recorded with a Perkin Elmer Spectrum GX spectrometer using a polarized wire grid (Perkin Elmer, MA, USA). For anisotropic meshes obtained using the rotating collector, the beam directed orthogonally to the specimen surface was polarized alternatively parallel or orthogonal to the longitudinal axis of the fibers, which allowed the influence of collector velocity on the P(VDF-TrFE) crystalline phase content to be evaluated. All the spectra were collected in the mid-IR region (4000–650 cm^{-1}) using 16 scans. The relative fraction of β-phase was calculated as:

$$F(\beta) = \frac{X_\beta}{X_\beta + X_\alpha} = \frac{A_\beta}{1.26A_\beta + A_\alpha} \tag{4}$$

where A_α and A_β correspond to absorption band intensities at 530 cm^{-1} and 840 cm^{-1} for α- and β- phases, respectively [34] (Supplementary Note 2).

XRD was also used to assess the amount of piezoelectric crystalline β-phase in the samples. XRD patterns were recorded on P(VDF-TrFE) fiber meshes (Siemens D500 Krystalloflex 810, Munich, Germany) using Cu Kα radiation (λ = 1.5406 Å) in reflection mode at a scanning rate of 0.03° s^{-1} with 2θ ranging in 0°-40° and a temperature of 25 °C.

DSC (TA Q200, New Castle, USA) was used to determine the Curie temperature (T_c), melting temperature (Tm) and crystalline content of electrospun fiber meshes. At the Curie temperature of ferroelectric materials such as P(VDF-TrFE), a ferroelectric to paraelectric state transformation takes place [35,36]. DSC experiments were performed by applying a heat-cool-heat temperature variation in the range from −70 °C to + 250 °C with heating rate 10 °C•min^{-1} and cooling rate 5 °C•min^{-1}, respectively. The crystallinity of samples was then calculated using the following relation:

$$X_c(\%) = \frac{H_{fs}}{H_{ft}} \times 100 \tag{5}$$

where H_{fs} is the measured heat of fusion to obtain the melting of the sample and H_{ft} is the heat of fusion for 100 % crystalline P(VDF-TrFE) (45 J•g^{-1}) [37] (Supplementary Note 2).

2.5. Mechanical properties

The scaffolds were characterized by a mechanical tester (INSTRON 5500R) equipped with MERLIN software (INSTRON, MA, USA). The load cell had a maximum capacity of 100 N, the crosshead speed was 5 mm•min^{-1}, whereas the length (2 cm) of the electrospun fiber sample was determined as the gap between the parallel sides of a paper frame, which was cut before starting the tests. An approximate cross-section area of each mesh was measured using a thickness gauge. Dynamic mechanical analysis (DMA) was carried out on a Gabo Eplexor® 100 N (Gabo Qualimeter® Testanlagen GmbH, Ahlden, Germany). A strip (~2 cm × 1 cm) was cut from the fiber mesh. A constant static stress and 1 % dynamic strain were applied in tensile mode. The tests were performed in the frequency range 5–100 Hz. Randomly selected scaffolds were tested and the results of three replicates ($n = 3$) were reported as mean and standard deviation.

2.6. Piezoelectric properties

Piezoelectric coefficients were measured, direct and converse, the latter in both longitudinal and transverse directions. In the first method (here named “pulsed direct piezo-tester”), fiber meshes, about 10 × 20 mm^2 area, were sandwiched between two aluminum foils and electric connections established by copper wires and silver paint. A thin film of polydimethylsiloxane was positioned on the top of each device to avoid sliding of the upper electrode and improve stability during electrical

characterization. A normal force was dynamically applied by an electromagnetically-driven piston (surface area 31.5 mm^2, applied pressure about 1.2 kPa) on the top of the upper electrode at a frequency of about 0.5 Hz. The output voltage (V_{out}) and current data were measured with a precision source-measure unit (Keysight B2911A) acquisition system. The input impedance during voltage measurements was set at 200 MΩ.

Piezoelectric transduction was also measured, according to our previous studies, using a home-designed set-up able to measure the converse, transverse piezoelectric coefficient d_{31} (here named "converse d_{31} piezo-tester") [4]. Briefly, a mesh strip with rectangular size about 20 × 5 mm^2 (x × y) was fixed by Teflon clamps to a holder, connected to a harmonic steel cantilever spring, and to a micro-translator to allow for sample pre-tension. An AC electric potential is applied in the transverse direction (z) through a pair of metal slabs, faced to the strip surface (xy), thus forming a capacitor. In this way, the transverse electric field produces a longitudinal stress (along x) in the sample, with a magnitude proportional to the d_{31} piezoelectric coefficient. The AC potential was chosen to match the resonant frequency of the steel cantilever, typically about 150 Hz, thus allowing the piezoelectric signal to be amplified by a typical factor of 20–30. An optical lever method was used to detect the bending of the cantilever, i.e., with a laser beam reflected by a mirror attached on the cantilever edge, and deflection detected by a four-quadrant split photodiode. The coefficient d_{31} was then calculated as:

$$d_{31} = 2.7 \times 10^4 \frac{\eta \varepsilon_S}{l_e} \frac{V_{out,RMS}}{Q_{sim}} \quad (6)$$

where η is the spacing between capacitor electrodes (1.5 mm), l_e is the electrode size along x axis (6.5 mm), $V_{out,\ RMS}$ is the vibration amplitude output, and

$$\varepsilon_s = \varepsilon_d - \frac{\eta_d}{\eta}(\varepsilon_d - 1) \quad (7)$$

is the effective dielectric constant experienced by our capacitor, where ε_d is the dielectric constant of P(VDF-TrFE), derived from the literature, and η_d the strip thickness normalized by its porosity. Q_{sim} is a factor relating the output of our measurement to the piezoelectric stimulation. It depends on the tensile spring constant k_s of the specimen and on the geometrical and physical parameters of our set-up; it is calculated using a mechanical model of the cantilever resonator, implemented in Mathematica software. Finally, the direct piezoelectric coefficient g_{31} was obtained as:

$$g_{31} = \frac{d_{31}}{\varepsilon_0 \varepsilon_d} \quad (8)$$

in which the dielectric constant of vacuum, ε_0, is $8.85 \cdot 10^{-12}$ $F \cdot m^{-1}$. Converse, longitudinal piezoelectric coefficient (d_{33}) and output voltage (V_{out}) of the samples were also measured by a YE2730A d_{33} meter and a cyclic direct PiezoTester, respectively (Supplementary Method S1).

2.7. Biological evaluation

Human MSCs were isolated from bone marrow aspirate residues of healthy adult patients undergoing routine total hip replacement surgery, after written consent, treated anonymously and in accordance with the principles expressed by Declaration of Helsinki. The local Ethics Committee of Area Vasta Nord Ovest (CEAVNO), Pisa, did not request any approval for this study, since it used completely anonymous surgical waste material. The successful hMSC isolation was performed according to well-established protocols [38]. Herein, the aspirate was diluted 1:3 (v/v) in sterile saline and layered on Lymphoprep as a density gradient. After centrifugation at 400 *g* for 25 min, the mononuclear cell layer was collected and cultured in low-glucose DMEM with 2 mM L-glutamine, 100 IU/mL penicillin, 100 mg/mL streptomycin and 10 % heat-inactivated FBS. After 48–72 h non-adherent cells were discarded, and fresh medium was added until 70–80 % confluence was reached. At this time, the adherent layers were trypsinized and seeded at low density (2000–3000 cells/cm^2) for further expansion.

The scaffolds fabricated with DMF/acetone and MEK at 500 rpm and 4000 rpm (size 1 × 1 cm^2) were sterilized in absolute ethanol for 24 h, then rinsed with three washes of 15 min with (PBS, 1 ×) containing 100 × penicillin/streptomycin and 100 × fluconazole. The cells used in this study were from passages 1–2. For each scaffold, 100,000 cells were resuspended in 20 μL of sterile-filtered 2 % (w/v) aqueous solution of gelatin, seeded on the top of the scaffold and incubated for 30 min at 37 °C in 24 well plates. Subsequently, 1 mL of cell culture medium was added to each well. The next day, in part of the samples, the cell culture medium was changed to osteogenic differentiation medium, which was replaced every 3 days. Osteodifferentiated and undifferentiated hMSC/scaffold cultures were carried out for 1 week ($n = 3$) for gene expression analysis.

The metabolic activity of the cells grown on the scaffolds was monitored in time using alamarBlue® assay. Data were acquired according to the manufacturer's instructions and expressed as the percentage of reduced alamarBlue® (%AB_{red}). Briefly, samples ($n = 3$) and negative controls ($n = 3$) were incubated for 3 h at 37 °C with the alamarBlue® dye diluted in culture media. At each time-point, i.e., 3 and 7 days, 100 μL of supernatant from sample or control was loaded into 96-well plates; then, excess supernatant was removed from the cultures and replaced with fresh culture media. The absorbance (λ) of supernatants was measured with a spectrophotometer (Victor 3; PerkinElmer, Waltham, MA, USA) under double-wavelength reading (570 nm and 600 nm). Finally, %AB_{red} was calculated by correlating the absorbance values and the molar extinction coefficients of the dye at the selected wavelengths, following the protocol provided by the manufacturer.

For gene expression analysis, total RNA was isolated from the osteodifferentiated hMSC/scaffold samples using TriReagent according to the manufacturer's protocol. The synthesis reaction of cDNA was performed with iScript cDNA Synthesis Kit starting from 50 ng of RNA in a total volume of 20 μl. The synthesis program included an initial incubation at 25 °C for 5 min, followed by incubation at 46 °C for 20 min. Reaction was inactivated heating at 95 °C for 1 min. To determine the expression of the selected genes, quantitative RT-PCR (qPCR) was performed on an CFX Connect Real Time System (Bio-Rad). In 20 μl final volumes, 2 × SsoAdvanced Universal SYBR Green Supermix, 400 nM primer and 5 ng total cDNA were used. The thermal protocol was applied with 1 cycle at 95 °C for 3 min for enzyme activation, followed by 40 cycles at 95 °C for 10 s and 60 °C for 30 s. Each assay included a "no template" sample and all tests were carried out in duplicate. Samples were analyzed by the 2-ΔΔCt method, as described by Livak and Schmittgen [39]. The relative expression of the target genes, namely, Runt-Related Transcription Factor 2 (RUNX2), Alkaline Phosphatase (ALPL), Osteopontin (OPN) and Osteocalcin (OCN), was normalized to the level of glyceraldehyde-3-phosphate dehydrogenase (GAPDH) as the selected housekeeping gene, in the same cDNA. Primers were designed with Beacon Designer Software v.8.0 (Premier Biosoft International, Palo Alto, CA, USA) with a junction primer strategy. The primer sequences of the investigated genes are reported in Table 1.

The scaffolds produced with MEK at 500 rpm and 4000 rpm ($n = 8$) were chosen to assess differentiation at a longer time-point, i.e., 14 days (i.e., 1 day in regular medium followed by13 days in osteogenic

Table 1
Primer sequences used for gene expression analysis via qRT-PCR.

Gene name	Forward	Reverse
GAPDH	CCCTTCATTGACCTCAACTACATG	TGGGATTTCCATTGATGACAAGC
RUNX2	GCCAAAAGGGTCATCATCTCTG	CATGCCAGTGAGCTTCCCGT
OPN	GCCGAGGTGATAGTGTGGTT	TGAGGTGATGTCCTCGTCTG
OCN	CTGTATCAATGGCTGGGAGCCCC	TGGTCAGCCAACTCGTCACAGTC
ALPL	GAGTATGAGAGTGACGAGAA	AGTGGGAGTGCTTGTATC

medium).

At the endpoint, the cell/scaffold constructs were washed twice with 1 × PBS and then fixed in 1 % (w/v) neutral buffered formalin for 10 min at 4 °C. The samples were subsequently rinsed with 1 × PBS and incubated with Osteoimage kit in order to detect mineralized matrix production. Samples were then counterstained with 10 μg/mL DAPI in 1 × PBS for 10 min at RT, to detect cell nuclei and washed in 1 × PBS. The specimens were observed by an inverted fluorescence microscope equipped with a digital camera (Nikon Eclipse Ti, Amsterdam, The Netherlands).

The calcium content in construct lysates ($n = 6$) was quantified using a colorimetric endpoint assay based on Arsenazo III. This assay measures the amount of blue/purple-colored Ca-Arsenazo^{2+} complex, formed when Arsenazo III binds to free Ca in an acid solution. The samples were incubated 1 N acetic acid overnight under shaking to allow calcium deposits to get efficiently into solution. The microplate was incubated for 10 min at RT before reading the absorbance at 650 nm in a plate reader (Victor 3; PerkinElmer).

For SEM analysis, fixed constructs were dehydrated in 70 % ethanol for 30 min and in absolute ethanol for 60 min; subsequently, they were incubated in a vacuum oven at 37 °C overnight, mounted on aluminum stubs, sputter-coated with gold (Sputter coater Emitech K550, Quorum Technologies Ltd, UK) and inspected using an FEI FEG-Quanta 450 system (Hillsboro).

2.8. Statistical analysis

Statistical analysis was carried out via GraphPadPrism software (version 6.0), using one-way ANOVA for parametric data was used. Analysis of multiple comparisons was performed with Tukey's aHonest

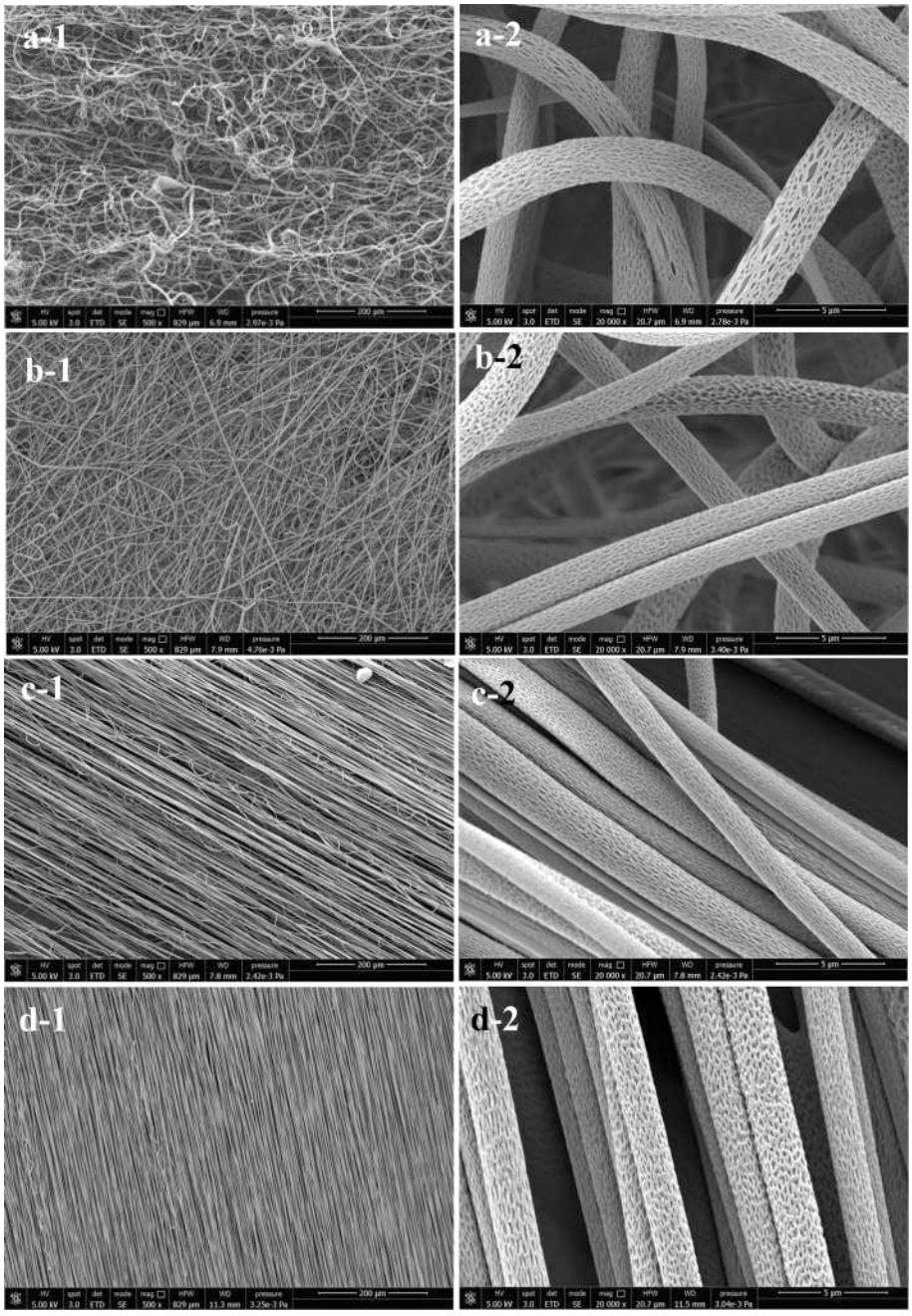

Fig. 1. SEM images of P(VDF-TrFE) fibers produced by electrospinning using MEK; Concentration: 20 wt%, voltage: 35 kV, tip-collector distance: 15 cm, flow rate: 0.016 mL·min^{-1}, collector velocity: 0 rpm (a), 500 rpm (b), 2500 rpm (c) and 4000 rpm (d). Different magnifications are shown in columns (1) and (2).

Significant Difference (HSD) test sa post-hoc test. Student *t*-test for paired data was used to compare the same samples' outputs over different time-points. Probability (p) values < 0.05 were considered as statistically significant.

3. Results

3.1. Scaffold morphological and physico-chemical characterization

The main goal of this research was the production of piezoelectric fibers with the desirable morphology and piezoelectricity to mimic the fibrillar and functional structure of collagen. At the first step of the study, the effect of the used solvent on morphology and piezoelectric properties of electrospun fibers produced at different collector velocities was investigated. The use of DMF/acetone led to the formation of fibers with undesirable morphological structure at all collector velocities investigated (Supplementary Fig. S1 and Supplementary Note 1), whereas the use of MEK gave rise to continuous ultrafine fibers provided with surface porosity in all production conditions (Fig. 1). The effect of RH on surface porosity of fiber meshes produced using MEK as a solvent is shown in Supplementary Fig. S2. Noticeably, decreasing RH to 26 % led to the formation of fibers with a completely smooth surface.

The rotating collector used in a velocity range of 0–500 rpm resulted in truly isotropic (random) fibers. Moreover, the higher velocity the better thickness uniformity along the width. Increased collector velocity from 2500 rpm to 4000 rpm led to the obtainment of evident anisotropic fibrous structures. Intermediate velocity regions (1000–2000 rpm) still had a non-oriented arrangement (data not-shown). The best fiber alignment was observed by using the highest collector velocity (4000 rpm). The collector velocity had a significant effect (p value ≤ 0.05) on fiber diameter (Table 2). Increasing collector speed up to 4000 rpm reduced the fiber diameter from 2.4 ± 0.6 μm to 1.3 ± 0.2 μm.

Scanning probe microscopy was employed to image at the nanoscale surfaces and structure of P(VDF-TrFE) fiber meshes (Fig. 2). To this aim, a fiber mesh produced by MEK was removed from the aluminum substrate used for fiber deposition, with the remaining filaments adhering effectively and then successfully imaged by AFM. Such fibers showed cylindrical symmetry, rough structure and regular surface porosity. Pores showed an oval shape with main dimensions in the order of few hundreds of nanometers and depth about hundred of nanometers (Fig. 2 b). Instead, electrospun meshes produced by the mixture of DMF/acetone were sticky, non-porous and could not be easily removed from the aluminum substrate to obtain isolated fibers suitable for AFM analysis (Supplementary Fig. S1 e). In addition, MEK produced fibers in reduced RH conditions had a non-porous surface (Supplementary Fig. S2 a).

The nano size distribution was evaluated on high magnification SEM micrographs. It highlighted that about or more than half (48-61 %) nanopores had an equivalent diameter size lower than 50 nm. The distribution of these pore sizes did not show to be related to the collector velocity. Rather, the eccentricity of the nanopores averagely (p = n.s.) increased with increasing the collector speed, reaching 0.971 ± 0.021 in the samples collected at 4000 rpm. The piezoelectric effect measured by the YE2730A d_{33} meter resulted higher for nanofibers produced using MEK as a solvent, for all collector velocities investigated (Supplementary Table S1). According to the morphology and the preliminary piezoelectric outcomes, fibers produced with MEK were selected for further studies. To compare the biological response of osteogenic cells, the best fiber scaffold types produced with MEK, in terms of morphology and piezoelectric properties, within the random and aligned types were chosen, namely, those obtained at 500 rpm and 4000 rpm, respectively, for an in-depth investigation. The porosity of the selected random (i.e., 500 rpm) and aligned (i.e., 4000 rpm) fiber meshes resulted 94 % ± 2 % and 85 % ± 2 %, respectively. The results of polarized FTIR on these scaffolds are reported in Fig. 3. It showed that there was not noticeable difference in the spectra of randomly oriented fiber mesh (i.e., 500 rpm) by using different incident beam polarizations, whereas aligned fibers (i.e., 4000 rpm) exhibited an increase in the intensity of bands associated with chain orientation (1076 cm^{-1} and 1400 cm^{-1}) for light polarized along their longitudinal axis.

Table 2
The effect of collector velocity on the diameter of fibers produced with MEK as a solvent.

Collector velocity (rpm)	0	500	2500	4000
Fiber diameter (μm)	2.4 ± 0.6	1.9 ± 0.5	1.4 ± 0.2	1.3 ± 0.2

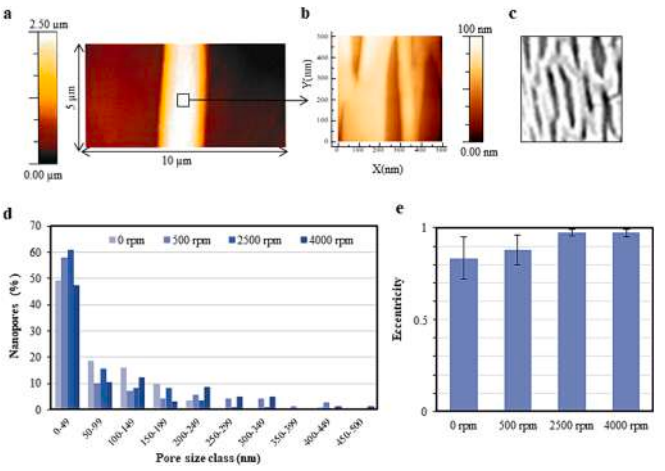

Fig. 2. Topographic analysis of P(VDF-TrFE) fiber surface produced with MEK: (a) AFM topography of single fibers, (b) AFM zoomed-in image of the fiber surface, (c) SEM zoomed-in micrograph of Fig. 1 d-2. Bar graphs showing: (d) nanopore size distribution according to equivalent diameter classes of 50 nm, and (e) eccentricity of the nanopore ellipsoid shape with increasing collector velocity (p = n.s.).

Increasing the collector velocity also led to an increase in the intensities of the crystalline bands representing β-phase (846, 884, 1124, 1181, 1285 and 1431 cm^{-1}) [37,38] (Supplementary Fig. S3 a). XRD and DSC results corroborated FTIR outcomes in terms of β-phase content and crystallinity (Supplementary Fig. S3 b,c, Supplementary Table S2, and Supplementary Note 2).

3.2. Scaffold mechanical characterization

The force–strain curves of fibers produced at collector velocities of 4000 rpm and 500 rpm are presented in Fig. 4 a, b. Results highlighted the significance of the alignment and role of straightened fibers on the mechanical properties of the meshes. In particular, the 4000 rpm fiber sample presented a nonlinear behavior described by a neo-Hookean model [41]:

$$\sigma = G\left(\lambda^2 - \frac{1}{\lambda}\right) + Y_0 \tag{9}$$

$$\lambda = 1 + \partial \tag{10}$$

where σ is stress, G is shear modulus of the sample, ∂ is strain and Y_0 is yield. Fitting of the nonlinear region of the stress–strain curve provided a value of G = 1.94 MPa and Y_0 = 4.55 MPa (Fig. 4 c). The force-strain curve of 500 rpm fiber meshes could not be compared to the previous one, since the sample underwent gradual fraying during pulling; therefore, the effective area gradually decreased while increasing strain, with consequent loss of proportionality between applied force and stress. A similar trend of results produced with DMF/acetone (Supplementary Fig. S4).

Further investigation of the mechanical behavior was performed by

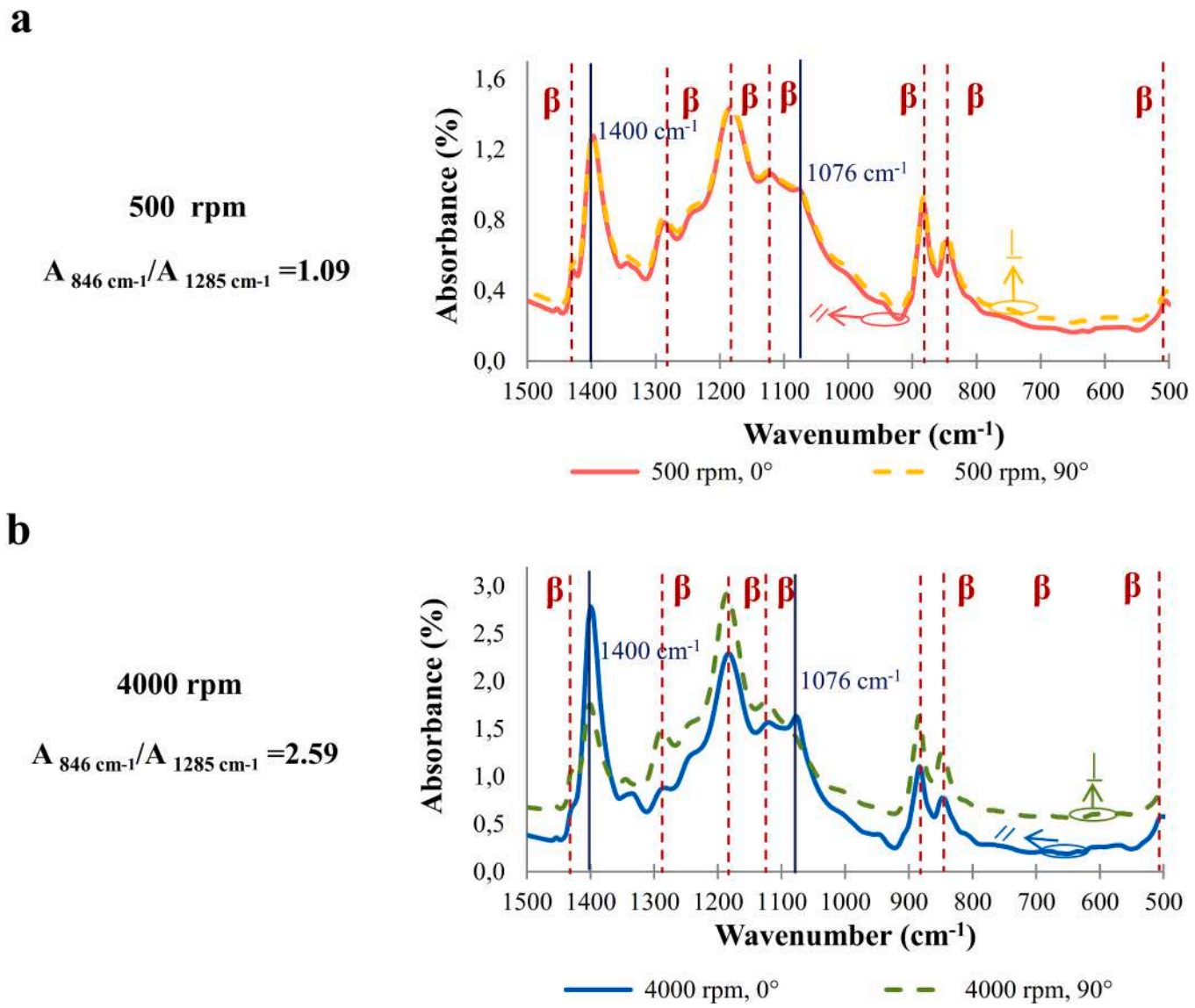

Fig. 3. FTIR spectra measured under different incident beam polarizations for: (a) randomly oriented (500 rpm), and (b) aligned (4000 rpm) fiber meshes. Light was polarized parallel and perpendicular to the main axis of the fiber.

DMA at RT in the frequency range of (5–100 Hz) and constant stress. The outcomes were presented in the form of storage modulus (E') (Fig. 5 a, b) and tanδ (Fig. 5 c, d), the latter being the ratio between the loss and storage moduli in a viscoelastic material, which provides a measure of damping. Under these working conditions, aligned electrospun fiber meshes exhibited higher storage modulus (120–140 MPa, increasing with frequency), compared to randomly oriented fibers (20–30 MPa). Tanδ was found to be about 0.1–0.2 over the applied frequency range.

The storage modulus at 100 Hz was also measured to obtain reliable values of the sample dynamic spring constant (k_{100Hz}) to be used in mechanical modeling for the "converse d_{31} piezo-tester". Such values resulted about 2–3 times higher than the static ones applicable with this piezo-tester (Table 3), thus, providing a significant correction to the resulting piezoelectric coefficients.

3.3. Scaffold piezoelectric characterization

Piezoelectric properties of electrospun fibers produced with MEK at collector velocities of 500 rpm and 4000 rpm were evaluated by means of two custom-made piezo-testers. Representative plots of the measured voltage and current signals, obtained by periodic compression by the "pulsed direct piezo-tester", are reported in Fig. 6 a,b. The plots show typical, periodic alternating negative and positive output peaks, corresponding to the application and release of the pressure pulse, with some uneven behavior in the positive and negative peaks, possibly associated to asymmetric compressive and recovery deformations of strained fibers during mechanical cycling. In the voltage profiles, a signal is caused by the compressive deformation of the sandwiched sheet of fibers and the opposite signal is recorded during the recovery deformation of the strained fibers while the piston recedes. Under such compressive cycles, fibers in random configuration were found to generate peak-to-peak voltages up to 4.2 V, corresponding to 110 nA currents, whereas fibers in aligned meshes were found to generate up to 3.1 V, corresponding to 42 nA currents. Finally, measurements of the converse piezoelectric coefficient d_{31} were also performed by "converse d_{31} piezo-tester", which took into the piezoelectric coefficient calculation the mechanical properties of the mesh. After equilibration under a load of 1 N for at least 12 h, the output of the piezo gauge was detected, and is shown in Fig. 6 (c), as a function of time after successive application of a DC potential of 0 V, +150 V, 0 V, −150 V, 0 V. The first part of the trace showed the spontaneous (i.e., remnant) piezoelectric effect, after which a positive potential of 150 V was applied, that increased the piezoelectric effect.

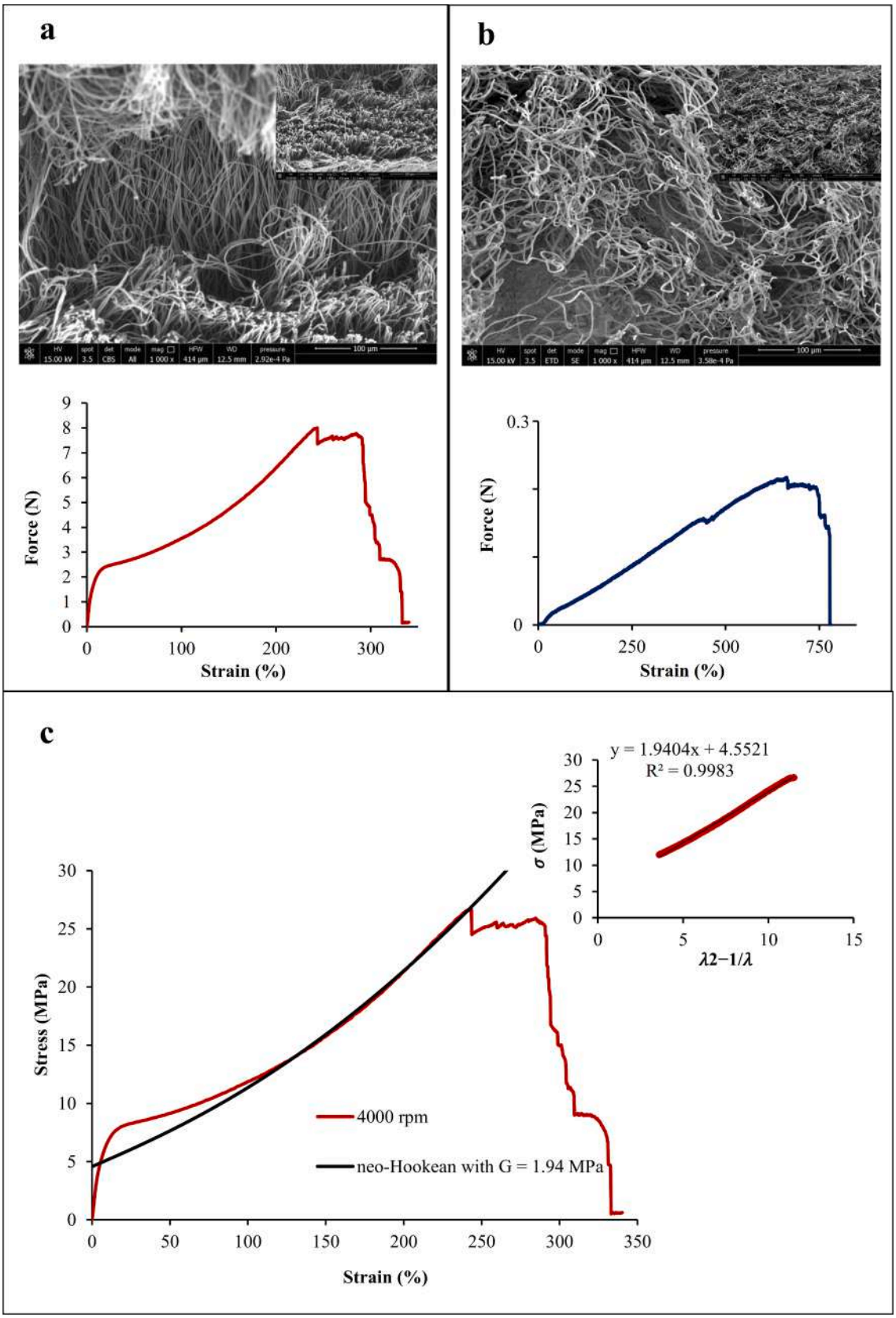

Fig. 4. Force-strain curves and cross-section SEM micrographs of P(VDF-TrFE) fiber meshes produced at collector velocities of: (a) 4000 rpm, and (b) 500 rpm; (c) Experimental and computed stress–strain curve for fibers produced at 4000 rpm.

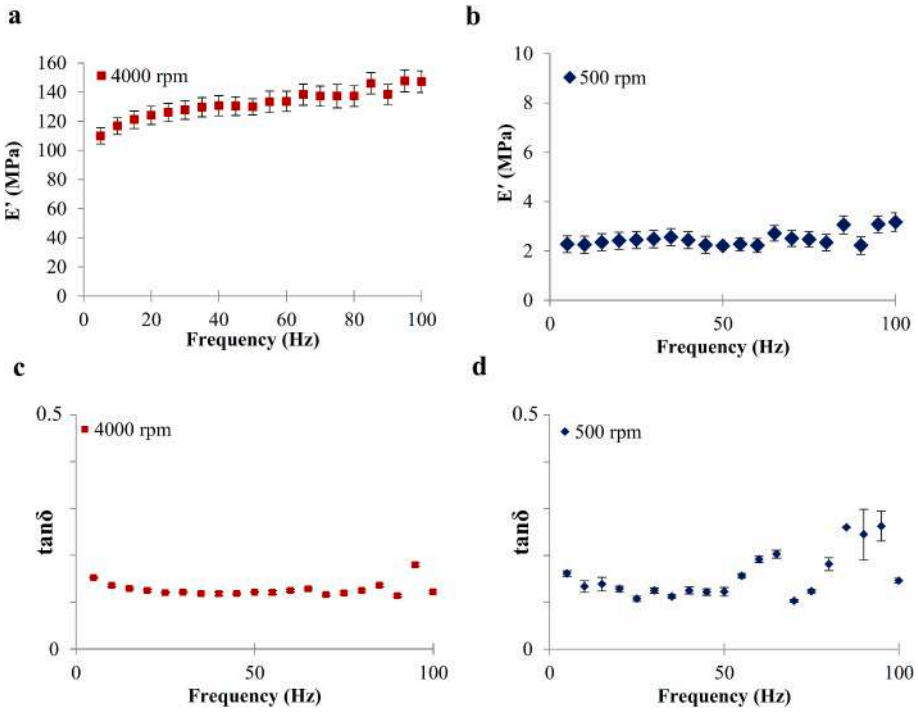

Fig. 5. DMA curves: (a, b) storage modulus (E'), and (c, d) tanδ of P(VDF-TrFE) fibers produced at collector velocities of 500 rpm and 4000 rpm at RT in the frequency range of 5–100 Hz and at constant stresses of 0.70 MPa and 2.94 MPa, respectively.

Table 3
Converse (d_{31}) and direct (g_{31}) piezoelectric coefficients of electrospun fibers produced by MEK. Specimen static spring constants, k_s, were measured *in situ* by the same setup, while dynamic k was derived from DMA measurements. Normalization factors Q_{sim} are carried out by a simplified analytical model of the mechanical response of the gauge.

Collector velocity (rpm)	ε_s	η_d (μm)	Static k_s (N·m^{-1})	Dynamic k_{100Hz} (N·m^{-1})	Q_{sim}	V_{out} (mV$_{RMS}$) (remnant – poled + 150 V – poled –150 V)	d_{31} (pm·V^{-1}) (remnant –poled + 150 V –poled –150 V)	g_{31} (m•V·N^{-1}) (remnant – poled + 150 V – poled –150 V)
500	11.5	44	1800	4000	5.3	1.1 ± 0.4 – 1.7 ± 0.4 – 3.5 ± 0.4	36 ± 13 – −55 ± 12 – 115 ± 13	0.34 ± 0.12 – 0.52 ± 0.11 – 1.08 ± 0.12
4000	11.5	44	3300	10,000	7.2	0.24 ± 0.14 – −0.89 ± 0.18 – 0.87 ± 0.19	5 ± 3 – −19 ± 4 – 19 ± 4	0.05 ± 0.03 – −0.18 ± 0.04 – 0.18 ± 0.04

Inversion of the DC potential led to a similar maximum piezoelectric effect with opposite phase, as expected. Corresponding values of converse piezoelectric coefficient, d_{31}, derived by Eq. (5), as well as of the direct coefficient, g_{31}, derived by Eq. (8), are reported in Table 3.

Minimum and maximum values are reported as "remnant" and "poled", respectively. The remnant d_{31} of fibers in random and aligned fiber meshes were 36 ± 13 pm•V^{-1} and 5 ± 3 pm•V^{-1}, respectively. The amount of poled (+150 V) d_{31} of random and aligned fiber meshes was −55 ± 12 pm•V^{-1} and −19 ± 4 pm•V^{-1}, respectively, while the amount of poled (−150 V) d_{31} ones was 115 ± 13 pm•V^{-1} and 19 ± 4 pm•V^{-1}, respectively. Positive control measurements on a commercial uniaxially stressed PVDF film (Goodfellow) provided d_{31} = 51 pm•V^{-1}, and negative control on a PTFE film provided d_{31} = 1.65 pm•V^{-1}, showed a sensible accuracy improvement of the d_{31} piezo-tester by better modeling of our gauge compared to previous works [4].

3.4. Scaffold biological characterization

Undifferentiated and osteodifferentiated hMSCs, were cultured on both random (i.e., 500 rpm) and aligned (i.e., 4000 rpm) fiber scaffolds for 7 days. The metabolic activity monitored over the culture time, as obtained with the AlamarBlue® test, is reported in Fig. 7.

In both undifferentiated and osteodifferentiated hMSC groups, the reduction percentage of the dye (% AB$_{red}$) at the culture endpoint was significantly higher in random ($p < 0.001$ and $p < 0.01$, respectively) than in aligned fiber scaffolds. A difference in hMSC metabolic activity was indeed visible soon at day 1 between random and aligned fibers, independently of cell differentiation ($p < 0.001$), whereas slight or no significance was found at day 1 in intra-material group comparisons ($p < 0.5$ within aligned and p = n.s. within random). At each time point, in each mesh type and differentiation group, the hMSCs were able to increase their metabolic activity with statistical significance, except for the undifferentiated hMSCs cultured on aligned fibers between day 4 and day 7. The highest metabolic activity among all the time points and groups was recorded in hMSCs osteodifferentiated on the random fiber scaffolds (45.24 % ± 6.12 %, $p < 0.001$). In the samples collected at 500 rpm and 4000 rpm osteodifferentiated for 6 days, the metabolic activity was similar by using both MEK and DMF/acetone (Supplementary Fig. S5a). A gene expression analysis, conducted on those samples preliminarly highlighted an increased expression in the samples collected at 500 rpm, although in most cases without statistical significance, of the osteogenic genes OPN ($p < 0.001$), RUNX2 ($p < 0.001$) and OCN (p = n.

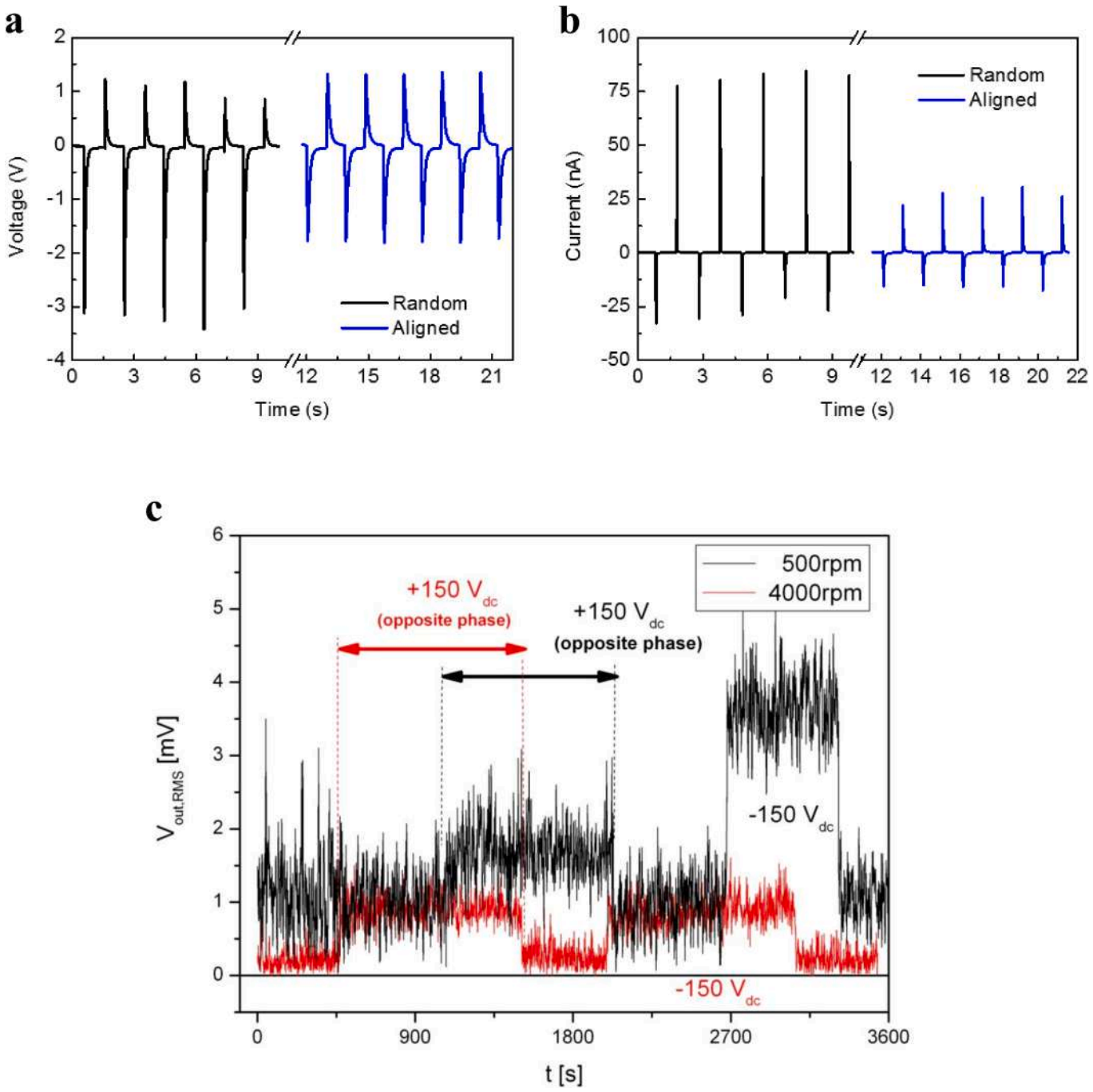

Fig. 6. Representative (a) Voltage-Time, and (b) Current-Time plots for the random and aligned porous PVDF-TrFE fibers under dynamic compression forces. (c) d_{31} piezoelectric response in different poling conditions. The response of the random fiber mesh (black) and of aligned fibers (red) is plotted as a function of time, for the following sequence of applied DC potentials: 0 V, +150 V, 0 V, −150 V, 0 V. Phase inversion of the AC signal is obtained for one of the DC potential polarities, meaning that the piezoelectric effect was inverted, as to be expected. (For interpretation of the references to colour in this figure legend, the reader is referred to the web version of this article.)

s.), as well as as well as ALPL (p = n.s.) and OCN (p = n.s.), with respect to those detected in the 4000 rpm counterparts (Supplementary Fig. S5b). The osteodifferentiation was performed on hMSCs cultured on MEK for 14 days, i.e., 13 days in osteodifferentiating conditions. At the timepoint, the samples were fixed, stained with DAPI and Osteoimage and observed under a fluorescence microscope.

Representative micrographs are displayed in Fig. 8. Cell nuclei were imaged in all the scaffolds, with abundance in the random meshes both for undifferentiated and osteodifferentiated hMSCs (Fig. 8 a,b), although many nuclei were also imaged in aligned meshes both for undifferentiated and osteodifferentiated hMSCs (Fig. 8 c,d), thus corroborating the metabolic activity results. The fluorescence staining confirmed that early osteogenesis occurred in the osteodifferentiated samples (Fig. 8 b,d), but the production of mineral matrix was more pronounced and defined in the random meshes (Fig. 8 b) than in the aligned counterparts (Fig. 8 d), as additionally corroborated via quantitative findings (Fig. 8 f).

All the fixed samples were post-treated for SEM imaging in order to assess cell morphology and fiber mesh colonization (Fig. 9). SEM analysis showed cells adhered to the fibers in all the culture conditions. In

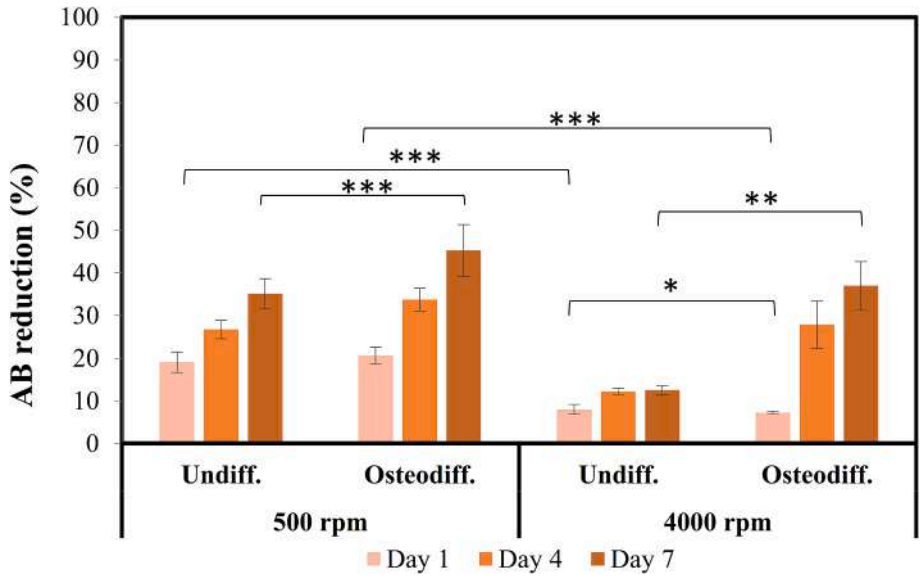

Fig. 7. Bar graph showing the results of metabolic activity of the samples monitored over 7-day culture time, as obtained via the AlamarBlue® test. Data are reported as mean ± standard deviation (* $p < 0.5$, ** $p < 0.01$, and *** $p < 0.001$).

the aligned fiber meshes, the undifferentiated hMSCs maintained a spindle shape morphology (Fig. 9 c), whereas, in the random fiber meshes, they displayed a cuboidal morphology typical of osteoblasts. Synthesis of mineral matrix deposition was clearly observed only in osteodifferentiated hMSCs on random fiber meshes, in which the osteoblastic morphology was well evident (Fig. 9 b). In the aligned samples, the osteoinduced hMSCs displayed a flat morphology without evident production of mineral matrix (Fig. 9 d).

4. Discussion

This study addresses hMSC osteodifferentiation on piezoelectric P (VDF-Tr-FE) electrospun fibers, by investigating the effects of different sovents, i.e., DMF/acetone and MEK, and different fiber configurations, i.e., random and uniaxially aligned. In particular, the samples were not subjected to mechanical forces during cell culture; thus, interesting results were obtained by the materials entitled with remnant piezoelectricy, namely, the randomly oriented ones. These findings may disclose novel routes for stimulating bone formation when the application of mechanical loads is not yet possible or insufficient, such us in bedridden and oteoporotic patients. Usually, many factors concur to an efficient cell-biomaterial interaction.

Along with topography, also mechanical and electrical properties of biomaterials employed as substrates for cell culture can provide cues that can be sensed by cells, thus enabling signals which will in turn define cell fate [42,43]. This is particularly evident when stem cells and materials with submicrometric features (namely, approaching subcellular features) are used, as the signals provided by the substrate can promote cell differentiation [43,44]. There is considerable interest in biomaterial-aided bone regeneration and repair in many orthopedic defects. Indeed, despite a large number of bone substitutes is available, the optimal clinical outcome is often challenging. New generation bone biomaterials are thus requested to act not only as mere mechanical and physical replacements, but they are expected to recapitulate the complex set of physiologic events involved in the biology of bone healing and formation [45]. Among others, the intriguing role exerted by collagen-driven bioelectricity on bone forming cells is not completely assessed [5]. Piezoelectric polymers can be processed into fibrous structures at a length scale which mimics the piezoelectric behavior of collagen fibrils and fibers of native ECM. So far, a limited number of studies face this salient topic, which have reported on the electromechanical effect of diverse PVDF-based 2D and 3D fibrous scaffolds and microspheres on bone formation by adipose-derived and bone marrow-derived hMSCs, and mainly focused on the application of dynamic loads, therefore releasing electrical output by mechanical inputs of diverse entities, e.g., vibrational and compressive [27,46,47]. In such a fragmented scenario, our research aims to better understand the role exerted by morphology and electric charge generation in piezoelectric electrospun scaffolds, so as to concur to developing effective therapies for bone repair and augmentation. Indeed, no real conclusion has been achieved on the best fibrous morphology, either random or aligned, for bone regeneration. It is a fact that many studies report on the best piezoelectric properties in aligned PVDF fibers [22,48], whereas, other biological studies on bone cells report on complex and diversified outcomes using non-electrically active random and aligned fiber scaffolds [49,50]. It has also to be considered that the optimal architectural features requested by neural cells, usually aligned fibers to have uniaxial morphological and electrical guidance [51], may not be as optimal for other cell types, including osteoblasts [49]. Indeed, bone ECM does retain a hierarchical structure, enabled by mechanically-driven orientations, which however develops through multiple steps, including remodeling. In addition, the combinational effect of fiber morphology and electric properties of biomaterials on bone regeneration is still unveiled.

In this study, fibrous piezoelectric P(VDF-TrFE) scaffolds were evaluated as substrates for early osteogenic differentiation of bone marrow-derived hMSCs without the application of any mechanical force, in order to assess the effect of scaffold morphology and the concomitant piezoelectric properties in rest mechanical conditions. This is important to determine the initial effect of the microenvironment, since, for example, bone fractures are usually treated in unloaded conditions in the first healing period [45]. Singularly, the type of scaffold morphology and the level of piezoelectric activity can indeed influence cell behavior at early stages (e.g., cell adhesion, cell growth and in turn, cell differentiation) [27,36]. However, the substrate morphology can also affect mechanical and piezoelectrical properties. To better understand the interplay between these properties, as they strongly depend on the fabrication parameters, the effect of solvent type and rotating velocity of the electrospinning collector on morphology, mechanical and piezoelectric properties of P(VDF-TrFE) fibrous meshes was investigated to select the optimally ECM-biomimetic substrate for *in vitro* culture of hMSCs. The obtained results demonstrated a significant effect of solvent

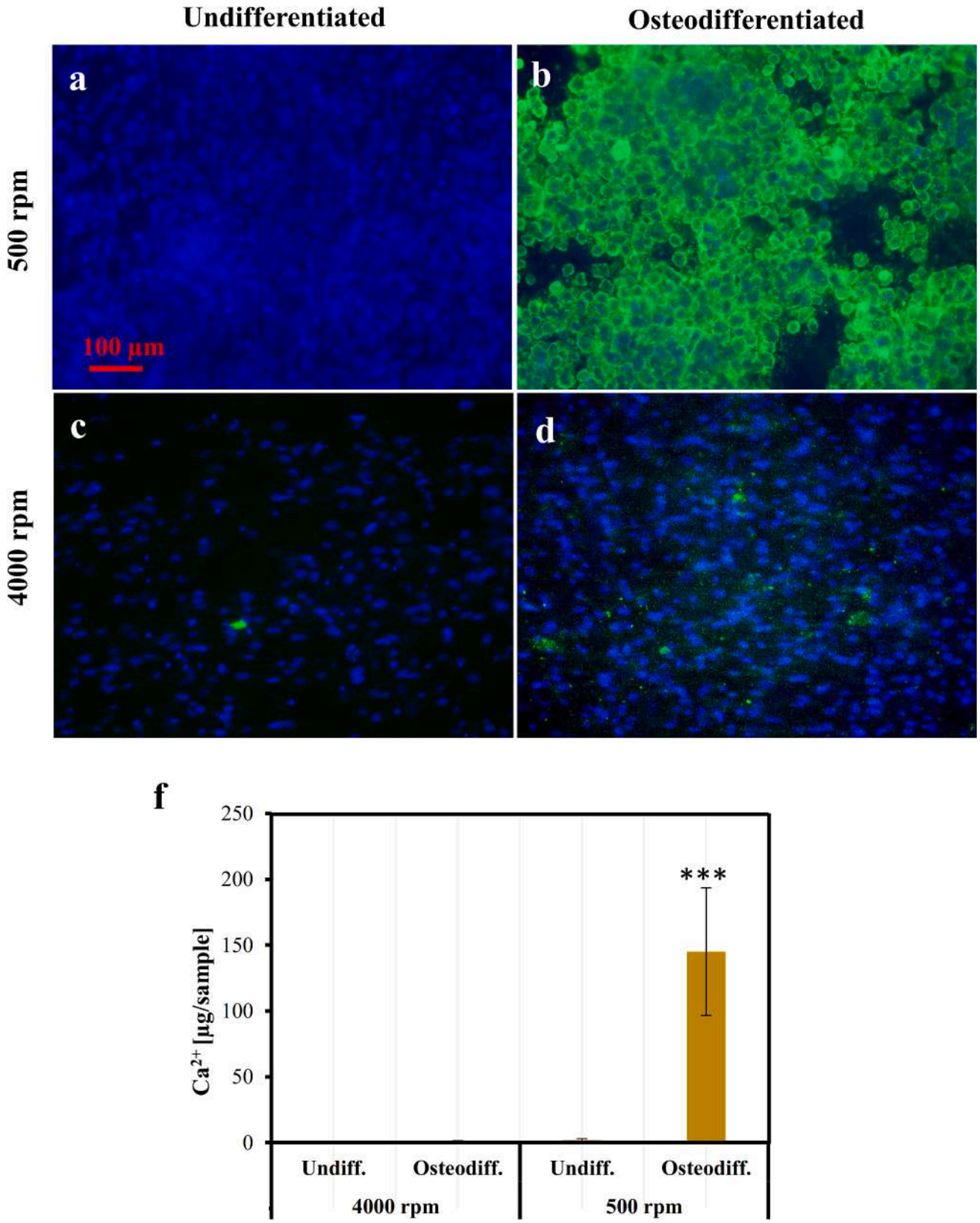

Fig. 8. Fluorescence staining (merged channels): DAPI in blue for cell nuclei, and Osteoimage in green for calcium matrix for (a, c) undifferentiated, and (b, d) osteodifferentiated hMSCs cultured on (a, b) random (i.e., 500 rpm), and (c, d) aligned (i.e., 4000 rpm) P(VDF-TrFE) fiber meshes for 14 days. Scale bar is the same (100 µm) for all the micrographs. (f) Bar graph showing calcium (Ca^{2+}) content per sample ($n = 6$); data as expressed as mean ± standard deviation (*** $p < 0.0001$). (For interpretation of the references to colour in this figure legend, the reader is referred to the web version of this article.)

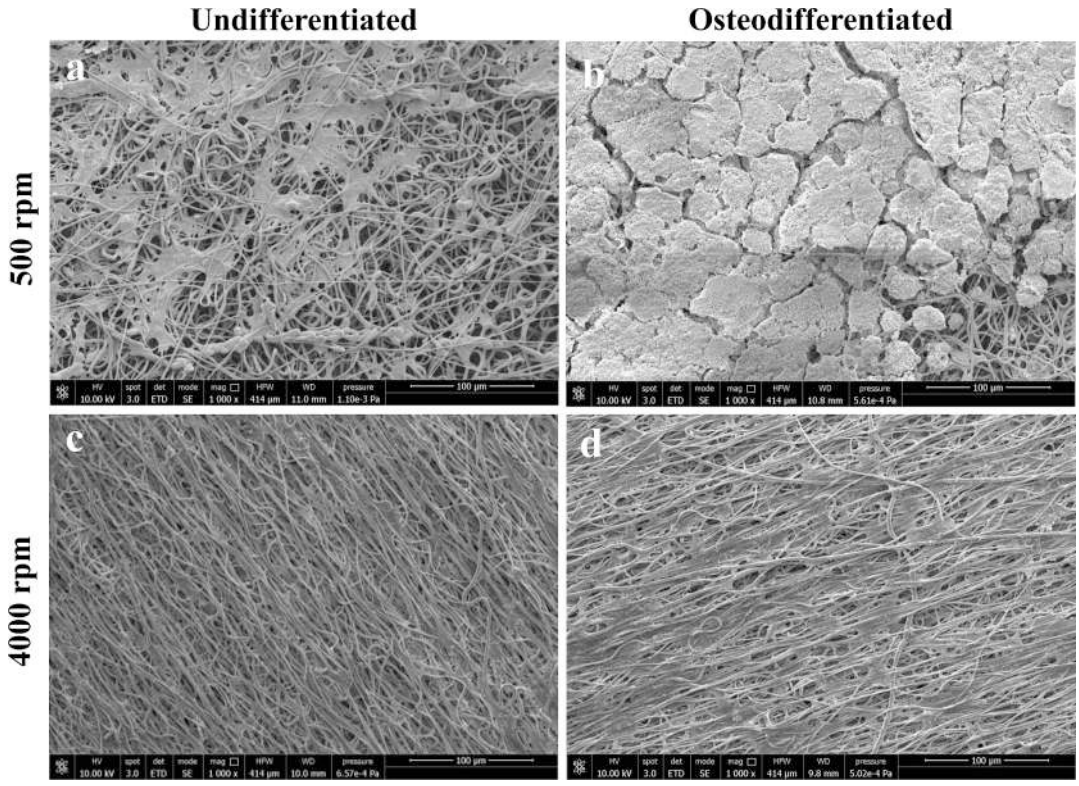

Fig. 9. SEM images of hMSCs cultured on (a, b) randomly oriented (i.e., 500 rpm), and (c, d) aligned (i.e., 4000 rpm) P(VDF-TrFE) scaffolds; (a, c) undifferentiated, and (b, d) osteodifferentiated hMSCs; 1000 × magnification, scale bar is 100 μm.

type and collector velocity on morphology and level of piezoelectric activity of electrospun fiber meshes. In our operational conditions, using DMF/acetone as a solvent mixture for P(VDF-TrFE) gave rise to overall melted fibrous meshes (with the static collector), up to smooth continuous fiber meshes still linked to each other by molten joint points (with the rotating collector). Differently, using MEK as a solvent in the same RH and temperature conditions, led to the formation of continuous ultrafine fibers provided with surface nanoporosity. Surface porosity can greatly enhance the surface area in ultrafine fiber meshes at a smaller length scale, thus providing additional cues for cell adhesion [52]. The formation of sticky structures and joints in fibers produced via DMF/acetone (1:1 v/v) can be related to the incomplete solvent evaporation in the jet traveling between the spinning tip and the surface collector due to the lower relative evaporation rate of this solvent mixture, which amounts to 3.16 [n-butyl acetate (nBuAc) = 1] [53].

Differently, using MEK as a solvent enabled higher relative evaporation rate of 4 (nBuAc = 1) with respect to DMF/acetone (1:1 v/v). Together with the environmental conditions (i.e., temperature, RH and pressure), an efficient solvent evaporation depends on the flight time of the fluid fiber before being collected, which also depends on the needle-to-collector distance and the interaction between the solvent(s) and the electric field. Higher electrical conductivity of polymeric solutions can also give rise to enhanced stretching during the electrospinning process and therefore the creation of uniform fibrous structures [54]. Among the many parameters that ultimately influence the fiber formation during the electrospinning process, thermodynamic and electrical properties of polymer solutions, namely, evaporation rate, boiling point, surface tension and dielectric constants, varied in our study by changing the solvent(s). However, polymer molecular weight, flow rate, working distance and environmental conditions were kept constant. Most importantly, applied voltage and polymer solution concentration, which are considered key factors impacting fiber size and morphology, were consistent between the DMF/acetone and MEK groups [55]. We can thus hypothesize that, in our working conditions, the thermodynamic and electrical properties of MEK altogether contributed to the formation of continuous and joint-free fibers. Our morphological investigation also indicated that the microstructure of electrospun fibers produced at the same RH, regardless of random or aligned orientation, varied from smooth to porous surfaces by changing solvent from DMF/acetone to MEK. Trapped MEK with moisture due to ambient RH (46 %) led to the formation of surface nanoporosity, which is desirable in bone tissue engineering for new ECM deposition, including mineralization [56]. The effect of humidity was demonstrated by reducing RH to 26 %, at which smooth fibers were obtained by using MEK. Further confirmation of surface texture of the fibers was obtained by AFM, highlighting the cylindrical geometry (average diameter of 2.4 ± 0.6 μm and 1.3 ± 0.2 μm for random and aligned fibers, respectively) and surface porosity of electrospun fibers produced by MEK at RH of 46 %, whereas DMF/acetone fibers appeared as smooth. These aspects are highly important; in fact, surface topography tailoring cell attachment and growth into fully functioning units has become a key research focus in tissue engineering [40]. The size of fiber nanopores was not affected by the collector speed. The nanopores had ellipsoid shapes and about half of the pores had equivalent diameter lower than 50 nm. Unlike nanopore size, eccentricity was increased by the rotating velocity. We thus showed that it was possible to develop nanoporous fiber surfaces by controlling the solvent used and the electrospinning humidity, finally obtaining nanopores with homogeneous size and highly eccentric elliptic shape. In addition, by modifying the scaffold surface structure, the ability of cells and proteins to adhere can be finely tuned. In addition to enhancing the alignment in the fiber arrays, the collector rotation at high velocity (> 2500 rpm) enabled the formation of denser electrospun fibers with uniform morphology and lower inter-fiber spacing (porosity = 85 % ± 2 %) in comparison to the randomly oriented fibers (porosity = 94 % ± 2 %) [57]. Also in this case, mesh porosity is an important factor in bone tissue engineering; typically, 90 % porosity allows a suitable microenvironment for osteoblast maturation [58]. A preliminary evaluation of piezoelectric coefficient d_{33} of the fiber meshes produced at different

collector velocities using the abovementioned solvent types was performed using a commercial equipment (YE2730A d_{33} meter) and allowed the identification of two main factors: (1) d_{33} increased with collector velocity in both groups, (2) the highest values were found using MEK. Basing on morphological and piezoelectric findings, MEK-produced scaffolds were thus selected for an extensive investigation. SEM results showed a considerable alignment in fiber mesh produced at 4000 rpm. The consequence of this arrangement is that overlapping of fibers is forced, thus reducing inter-fiber porosity, increasing volumetric density and eventually enhancing the mechanical properties of the fiber meshes. FTIR, XRD and DSC analyses showed that the highest collector velocities also caused the electrospun fibers being effectively stretched to form highly oriented β-phase crystallites with a slight increase in the degree of total crystallinity.

Weber *et al.* have stated that electrospinning enhances crystallinity, Xc (%) and the amount of the polar β-phase crystallites, if compared to the unprocessed P(VDF-TrFE) powder [36]. During electrospinning, two relevant forces are applied to the polymeric solution: a shear force when it flows through a needle, and a Columbic force when the high electric field elongates and accelerates the jet. Using a rotating collector adds a mechanical pulling force. The abovementioned three forces may cause alignment in polymer chains and/or stretching them in the spinning direction, thus they are invoked to induce the polar β-phase formation through the gauche conformation change to the straighter all-trans conformation [59]. At high collector velocities, the β-phase may significantly be favored by the mechanical force exerted by the rotating collector. DSC results supported the conclusion that for the highest collector velocity used in our study (i.e., 4000 rpm), orientation and packing of the polymer chains were facilitated, as also shown by the increase of Curie transition enthalpy of β-phase (F_β) Supplementary Note 2.

Studying the resulting mechanical behavior of fibrous meshes is also highly important for evaluating the concurrent effect on the piezoelectric properties, as well as their possible applications in tissue engineering [60]. On a microscopic scale, the scaffold should be rigid enough to support cell adhesion and spreading. Simultaneously, on a macroscopic scale, the scaffold must have mechanical properties suitable for the target tissue. Even though the mechanical properties of porous polymers cannot match those of bone, fibrous meshes can be potentially incorporated inside matrices to create bio-synthetic composites, thus replicating the structure of bone, in which collagen fibers are incorporated within a mineral (e.g., ceramic) matrix [56]. In our work, we have evaluated the mechanical properties of random and aligned fiber meshes. In isotropic meshes, mechanical testing basically takes into account the fiber–fiber contact points, since it is difficult to have fibers going from one grip of the tensile tester all the way to the other, which instead predominantly occurs in the case of aligned fibers. Therefore, normalization of the specimen section by material density was not considered reliable in this comparative study. As such, the cross-section area of each fiber ribbon was estimated. Accordingly, the results of the tensile tests were finally reported as apparent Young's moduli and apparent tensile strengths. The structural properties of electrospun fibers, including fiber diameter, molecular alignment level of the polymeric chain within a fiber and degree of alignment of fibers, all have an important effect on tensile properties. The mechanical behavior of fiber meshes is also closely linked to their crystalline morphology, which leads to different behaviors at the amorphous-crystalline interfacial regions [61]. The arrangement of the polymer chains, including alignment, affects the ability of fiber meshes to resist deformation (i.e., tensile strength) [62,63]. By using a simple dynamical mechanical stretching process on P(VDF-TrFE) fibers obtained under low rotation speed, Ma *et al.* have enabled the formation of large-scale highly oriented electrospun fibers with enhanced mechanical and piezoelectric properties [64]. In our study, aligned P(VDF-TrFE) fibers showed a relevantly higher tensile strength than random ones. Good fitting of the Neo-Hookean model with the stress–strain curve of our aligned fibers indicated that a larger external stress is required to unfold polymer chains within the fibers, in comparison with randomly oriented fiber meshes.

Randomly oriented fiber meshes showed a larger elongation than that of aligned fibers. Kumar *et al.* have concluded that introducing some degree of orderliness in a fiber mesh not only increased the strength of the material, but also affected its extensibility through the higher apparent Young's modulus [62]. Such a behavior may be due to the instantaneous participation of a large number of fibers during tensile testing. On the other hand, when the fibers are oriented in the stretching direction, their uniaxial architecture helps the tensile force to distribute equally across the sample [4]. In good agreement with the above results, our results of DMA showed that aligned fibers had higher storage modulus than that of the randomly oriented fibers. Under these working conditions, P(VDF-TrFE) fiber strips had moderately viscoelastic behavior. Over the applied frequency range, tanδ of electrospun fibers was obtained in the range 0.1–0.2, thus supporting the fact that these fibers had no predominant viscous effects at RT. Analogously to the P(VDF-TrFE) fiber produced using MEK as a solvent, the mechanical findings of the fibers produced with DMF/acetone as a solvent system, underscored the pivotal role of alignment degree. Once more, the 4000 rpm fiber specimen exhibited a nonlinear behavior, fitting well with a neo-Hookean model. The application of this model to the nonlinear segment of the stress–strain curve yielded values of $G = 1.30$ MPa and $Y_0 = 0.34$ MPa.

Diverse methods based on different geometries and excitation mechanisms were used to investigate the piezoelectric properties of the samples, including d_{33}, d_{31} and generated voltage V_{out}, for samples produced with the two different solvent types and as a function of collector velocity. Due to the complex structure of the fibrous meshes, which affects the piezoelectric behavior of the samples, no trivial relation is generally expected among the different piezoelectric coefficients. Mechanical properties of fiber meshes, such as material stiffness, have significant effects on the overall charge separation, and therefore the piezoelectric performance [50]. To consider the effect of mechanical properties of the 500 rpm and 4000 rpm produced fiber meshes on piezoelectric coefficient measurement, the converse d_{31} piezo-tester was used with the ability to measure converse piezoelectric coefficient of pristine samples, in absence of any mechanical stimulation that could induce poling in the material, as well as during a temporary poling induced by an external electric field. The minimum value reported indicated a spontaneous (or remnant) piezoelectric effect, obtained after equilibration of the fiber mesh. Such an equilibration was necessary to obtain repeatable results, since any mechanical stress applied to the sample, as for instance during sample fixing to the piezo-tester gauge and pre-tensioning, had the tendency to cause some mechanically induced poling, and therefore piezoelectric activity, that nevertheless was observed to decay with a characteristic time of about 10 min. Moreover, several hours were needed to reach the situation in which deformation of the sample had enough small rates to allow measurements in constant stress conditions to be performed.

Remnant polarization is a peculiar characteristic of ferroelectric materials, which exhibit a residual non-zero polarization value even in the absence of external electric fields. The direction of remnant polarization can be reversed by the application of a strong electric field exceeding the so-called coercive field. Small values of remnant polarization in ferroelectric PVDF copolymers can be explained in terms of the disordered arrangement of their ferroelectric β-phase crystallites within the as-produced material, which tends to cancel out global polarization by a greater extent. Remnant polarization and piezoelectric coefficients can be increased by applying specific poling procedures, involving mechanical strain and/or strong electric fields during thermal annealing [27]. The simultaneous application of a DC potential tended to increase the piezoelectric effect because of a temporary poling effect, probably favoring the orientation of ferroelectric crystallites, or even the fibers themselves, along the electric field direction. By removing the DC

potential, the remnant piezoelectric effect was recovered. Such an effect was also found previously in similar systems [4].

Values of both remnant and poled piezoelectric effect resulted higher in the randomly-oriented than in the aligned fiber meshes, probably due to the possibility of fibers spun at low collector velocity to be aligned by the external electric field, which became the dominant force with respect to mechanical stretching, during both electrospinning and d_{31} measurement.

As noted by other studies, the level of piezoelectricity can influence cell growth and in turn MSC osteogenic differentiation, ultimately affecting mineralization and osteogenic gene expression under dynamic culture conditions [27,65]. In our biological analysis using bone marrow-derived hMSCs, the *in vitro* studies at 7 days showed that in rest mechanical conditions, cell viability (measured in terms of metabolic activity) was better in 500 rpm samples, including undifferentiated and osteodifferentiated hMSCs. The preferential capability of supporting hMSC adhesion by random fibers was shown soon on day 1, and consequently affected the growth timeline. In our samples, the structural organization of the fibers changed along with mesh porosity and slightly with fiber diameter; however, due to the low pore size of the meshes (in the order of few tens of μm) if compared to the hMSC size (in the order of 100 μm) and to thin thickness of the meshes used for cell cultures (about 300 μm), this phenomenon is not expected to deal with any oxygen limitations as sometimes observed in 3D scaffold culture [66]. Conversely, inter-spatial organization of fibers was the most evident and crucial factor when comparing random versus aligned fiber meshes. The random organization of fibrous non-piezoelectric polymeric scaffolds, both electrospun (sub-to-few μm size fibers) and dry-wet spun (hundred μm size fibers) has interestingly shown to affect hMSC osteodifferentiation by increasing alkaline phosphatase (ALP) activity, an early osteogenic marker [49,67]. However, in those non-piezoelectric materials such findings were not related to evidence of improved mineralization. In the work of Lyu and coworkers, in fact, the highest mineralization was finally found on aligned fiber meshes, which were proposed for periosteum regeneration [49]. Recently, another study has reported an enhanced proliferation by pre-ostoblasts (rat MC3T3-E1 cells) on perfectly aligned P(VFD-TrFE) fiber membranes under sinusoidal dynamic stimulation, as a remarkable example of bone cell sensitivity to piezoelectric properties [65]. We investigated the expression of the osteogenic lineage genes, such as RUNX2, ALPL, OPN and OCN, in hMSCs osteoinduced for 6 days, upon culture on P(VDF-TrFE) scaffolds produced using either MEK or DMF/acetone. The obtained outcomes were suggestive of an increased gene upregulation in the 500 rpm samples with respect to the 4000 rpm counterparts [68]. The influence played by architectural and electric features on stem cell fate is still unclear and deserves extensive investigation. In our outcomes, randomly oriented electrospun fiber meshes better promoted osteogenic differentiation of hMSCs after 13 days, in comparison to aligned fiber meshes, as confirmed by morphological imaging showing cuboid cells within abundant calcium matrix and by quantitative data, indicating 145 ± 48 μg Ca^{2+} production per sample by osteodifferentiated hMSCs cultured on random scaffolds. Due to the fibrous net and the larger inter-fiber spaces of random fiber meshes, as confirmed by porosity values, hMSCs could have found a proper 3D cellular organization, thus facilitating their morphological change from spindle- into cuboid-like morphotype, as an additional driving force for osteogenic commitment. Other factors, such as higher cell density found at the end-point, could have promoted the osteodifferentiation signaling cascade. In addition, it is important to stress that the random P(VDF-TrFE) scaffolds assayed in this study retained residual piezoelectricity in static conditions, which could have determined, concomitantly with morphology, an enhanced osteogenic differentiation responsiveness of hMSCs in terms of calcium matrix deposition. Nevertheless, it is reasonable and in line with bone biology that at later osteogenic stages (e.g., pre-osteoblasts) and/or in presence of mechanical stimulation, aligned piezoelectric fibrous structures could better mimic and promote bone formation as they are more representative of mature bone collagen fibers [68].

These *in vitro* findings suggested that the combination of morphological traits and piezoelectric activity in P(VDF-TrFE) scaffolds may promote the osteodifferentiation of hMSCs in a controlled manner by acting at the early stages of bone formation in unloaded conditions, which could be useful for the development of orthopedic therapies in difficult bone defects, which require patients' immobilization for certain periods.

As also previously reported [5], a number of mechanisms of electric nature have been proposed to be responsible for cell stimulation. Piezoelectricity was the first mechanism to be put forward since the assessment of dry bone piezoresponse. However, hydrated bone showed remarkably different behaviors, entailing the presence of other mechanisms, as for instance the possible semiconductivity arising at the apatite/collagen interface, or the action of streaming potentials, due to flow of ion-containing interstitial fluids due to pressure. Additionally, changes in electric potential of the extracellular environment could affect cell response due to the related perturbation of the transmembrane potential. Electrospun, porous nanofibers exhibiting piezoelectricity have a twofold function, namely, promoting cell adhesion to their porous structure as well as in the interspaces among the fibers comprising the mesh, as well as producing surface charge, located in close contact with the cell membrane, due to deformation related to cell development, by mimicking the behavior of bone tissue. A positive feedback mechanism could be envisaged for P(VDF-TrFE) and ferroelectric nanostructures in general, where remnant electric charges present at the surface of ferroelectric ultrafine fibers could provide electrical cues for cell growth, while the cell movements could produce further electrical polarization of the fibers due to their piezoelectric yield. Randomly oriented fibers could thus be more effective than aligned ones, for their higher mobility and possibility to be deformed by the pressure exerted due to cell growth, because of the lesser constrained structure, compared to that of aligned fibers, which can be deformed with limited degrees of freedom.

Even though not fully elucidative up to now, several evidences have highlighted the prominent role of electric signals in stem cell osteodifferentiation. It is highly expected that the application of piezoelectric biomaterials can guide bone tissue regenerative processes led by stem cells in a biomimetic fashion, considering the additional abilities of piezoelectric materials to improve vascular and neural functions [69–71].

5. Conclusion

The underlying idea of using piezoelectric scaffolds for bone tissue engineering relies on the fabrication of synthetic microenvironments, which offer physiologic-like stimuli to the cells, such as electric signals, as occur in the native tissue. The electrospinning method was used to produce thin meshes of P(VDF-TrFE) fibers. The effect of two types of solvents and different collector velocities on the morphology, mechanical and piezoelectric properties of electrospun fibers was investigated. MEK was finally selected to produce optimal scaffolds, provided with surface nanoporosity. Increasing collector velocity up to 4000 rpm reduced fiber diameter and porosity, whereas it improved fiber alignment, mechanical properties and piezoactive β-phase of the scaffolds. The electrospun fiber meshes displayed an elastic behavior with moderate viscous dissipations up to 100 Hz frequency. Interestingly, increased remnant piezoelectricity was assessed in the scaffolds produced at 500 rpm, namely in the form of randomly aligned fibrous meshes (i.e., produced at 500 collector velocity), with respect to the uniaxially aligned ones (i.e., produced at 4000 rpm collector velocity). Finally, *in vitro* tests performed using hMSCs in static culture conditions confirmed the good cytocompatibility of P(VDF-TrFE) fibrous scaffolds and specifically showed a significantly higher osteogenic differentiation in the random fiber meshes if compared to the aligned counterpart. We hypothesize that a concomitant effect of scaffold morphology (including

porosity and isotropic architecture) affecting preliminary steps like cell adhesion and morphology, together with residual piezoelectricity, could have promoted the early osteogenic differentiation cascade in hMSCs. Therefore, such substrates are promising for hMSC growth and osteogenic differentiation in the early stages of bone formation, with interesting potential for bone tissue engineering applications.

Competing interests

The authors declare no competing interest.

CRediT authorship contribution statement

Bahareh Azimi: Writing – original draft, Methodology, Investigation, Data curation. **Massimiliano Labardi:** Writing – review & editing, Writing – original draft, Methodology, Investigation, Formal analysis, Data curation, Conceptualization. **Mohammad Sajad Sorayani Bafqi:** Visualization, Investigation. **Teresa Macchi:** Data curation, Investigation. **Claudio Ricci:** Formal analysis, Software. **Veronica Carnicelli:** . **Lorenzo Scarpelli:** Investigation. **Istiak Hussain:** Investigation. **Francesca Matino:** Investigation, Data curation. **Michelangelo Scaglione:** Methodology, Resources. **Dario Pisignano:** Supervision, Resources. **Andrea Lazzeri:** Resources. **Mohammed Jasim Uddin:** . **Luana Persano:** Writing – review & editing, Writing – original draft, Validation, Resources, Methodology, Formal analysis, Data curation. **Serena Danti:** Writing – review & editing, Writing – original draft, Methodology, Funding acquisition, Conceptualization, Project administration, Supervision.

Declaration of competing interest

The authors declare that they have no known competing financial interests or personal relationships that could have appeared to influence the work reported in this paper.

Data availability

Data will be made available on request.

Acknowledgments

The authors gratefully acknowledge the MIT-UNIPI project "NANOSPARKS" (MISTI funds 2016) supported by Massachusetts Institute of Technology (MIT) and University of Pisa (UNIPI) for improving piezoelectric fiber research. The Centre for Instrumentation Sharing - University of Pisa (CISUP) is acknowledged for SEM analysis. Dr. Antonella Manariti (University of Pisa, Italy) is acknowledged for her technical support to FTIR analysis, Prof. Stefano Berrettini is acknowledged for hosting cell culture research at OtoLab (Azienda Ospedaliero-Universitaria Pisana, Italy). Dr. Delfo D'Alessandro and Dr. Luisa Trombi (University of Pisa) are gratefully acknowledged for technical support to cell culture and biological analysis. Ms. Aurora Magnani (University of Pisa) and Ms. Isabelle Su (Massachusetts Institute of Technology) are acknowledged for supporting the fabrication some fiber mesh samples and for their help with d_{31} piezo coefficient measurements, respectively. Finally, the authors thank Prof. Sara Filippi (University of Pisa) and Prof. Ranieri Bizzarri (University of Pisa) for their technical and logistic support for XRD and RT-PCR analyses.

Appendix A. Supplementary material

In the supporting information: morphological and piezoelectric data about acetone/DMF-produced fibers, the effect of RH on MEK-produced fibers, and P(VDF-TrFE) crystallinity of MEK-produced fibers via FTIR, XRD, DSC analyses, mechanical properties of DMF/acetone fibers, metabolic activity and gene expression analysis of DMF/acetone and MEK fibers cultured with osteodifferentiated hMSCs are reported. Supplementary data to this article can be found online at https://doi.org/10.1016/j.matdes.2024.112973.

References

[1] B. Thavornyutikarn, N. Chantarapanich, K. Sitthiseripratip, G.A. Thouas, Q. Chen, Bone tissue engineering scaffolding: computer-aided scaffolding techniques, Prog. Biomater. 3 (2–4) (2014) 61–102.
[2] C. Ribeiro, D. Correia, I. Rodrigues, L. Guardao, S. Guimaraes, R. Soares, S. Lanceros-Mendez, In vivo demonstration of the suitability of piezoelectric stimuli for bone reparation, Mater. Lett. 209 (2017) 118–121.
[3] C. Halperin, S. Mutchnik, A. Agronin, M. Molotskii, P. Urenski, M. Salai, G. Rosenman, Piezoelectric effect in human bones studied in nanometer scale, Nano Lett. 4 (7) (2004) 1253–1256.
[4] C. Mota, M. Labardi, L. Trombi, L. Astolfi, M. D'Acunto, D. Puppi, G. Gallone, S. Berrettini, L. Bruschini, S. Danti, Design, fabrication and characterization of composite piezoelectric ultrafine fibers for cochlear stimulation, Mater. Des. 122 (2017) 206–219.
[5] A.H. Rajabi, M. Jaffe, T.L. Arinzeh, Piezoelectric materials for tissue regeneration: A review, Acta Biomater. 24 (2015) 12–23.
[6] C. Ribeiro, V. Sencadas, D.M. Correia, S. Lanceros-Méndez, Piezoelectric polymers as biomaterials for tissue engineering applications, Colloids Surf. B Biointerfaces 136 (2015) 46–55.
[7] S. Danti, G. Ciofani, G. Pertici, S. Moscato, D. D'Alessandro, E. Ciabatti, F. Chiellini, M. D'Acunto, V. Mattoli, S. Berrettini, Boron nitride nanotube-functionalised myoblast/microfibre constructs: a nanotech-assisted tissue-engineered platform for muscle stimulation, J. Tissue Eng. Regen. Med. 9 (7) (2015) 847–851.
[8] P. Martins, A.C. Lopes, S. Lanceros-Mendez, Electroactive phases of poly (vinylidene fluoride): determination, processing and applications, Prog. Polym. Sci 39 (2014) 683–706.
[9] S. Martino, F. D'Angelo, I. Armentano, J.M. Kenny, A. Orlacchio, Stem cell-biomaterial interactions for regenerative medicine, Biotechnol. Adv. 30 (1) (2012) 338–351.
[10] J. Fang, H. Niu, H. Wang, X. Wang, T. Lin, Enhanced mechanical energy harvesting using needleless electrospun poly (vinylidene fluoride) nanofibre webs, Energ. Environ. Sci. 6 (7) (2013) 2196–2202.
[11] S.M. Damaraju, S. Wu, M. Jaffe, T.L. Arinzeh, Structural changes in PVDF fibers due to electrospinning and its effect on biological function, Biomed. Mater. 8 (4) (2013) 045007.
[12] S. Sharma, Ferroelectric nanofibers: Principle, processing and applications, Adv. Mater. Lett 4 (2013) 522–533.
[13] C. Ribeiro, D.M. Correia, S. Ribeiro, V. Sencadas, G. Botelho, S. Lanceros-Méndez, Piezoelectric poly (vinylidene fluoride) microstructure and poling state in active tissue engineering, Eng. Life Sci. 15 (4) (2015) 351–356.
[14] M.S.S. Bafqi, R. Bagherzadeh, M. Latifi, Fabrication of composite PVDF-ZnO nanofiber mats by electrospinning for energy scavenging application with enhanced efficiency, J. Polym. Res. 22 (7) (2015) 130.
[15] D.M. Correia, R. Gonçalves, C. Ribeiro, V. Sencadas, G. Botelho, J.G. Ribelles, S. Lanceros-Méndez, Electrosprayed poly (vinylidene fluoride) microparticles for tissue engineering applications, RSC Adv. 4 (62) (2014) 33013–33021.
[16] Z. Li, C. Wang, One-dimensional nanostructures: electrospinning technique and unique nanofibers, Springer, 2013.
[17] S. Agarwal, J.H. Wendorff, A. Greiner, Use of electrospinning technique for biomedical applications, Polymer 49 (26) (2008) 5603–5621.
[18] A. Gheibi, M. Latifi, A.A. Merati, R. Bagherzadeh, Piezoelectric electrospun nanofibrous materials for self-powering wearable electronic textiles applications, J. Polym. Res. 21 (7) (2014) 469.
[19] C. Ribeiro, V. Sencadas, J.L.G. Ribelles, S. Lanceros-Méndez, Influence of processing conditions on polymorphism and nanofiber morphology of electroactive poly (vinylidene fluoride) electrospun membranes, Soft Mater. 8 (3) (2010) 274–287.
[20] V. Sencadas, C. Ribeiro, I. Bdikin, A. Kholkin, S. Lanceros-Mendez, Local piezoelectric response of single poly (vinylidene fluoride) electrospun fibers, Physica Status Solidi (a) 209 (12) (2012) 2605–2609.
[21] F. Huang, Q. Wei, Y. Cai, N. Wu, Surface structures and contact angles of electrospun poly (vinylidene fluoride) nanofiber membranes, Int. J. Polym. Anal. Charact. 13 (4) (2008) 292–301.
[22] W.A. Yee, A.C. Nguyen, P.S. Lee, M. Kotaki, Y. Liu, B.T. Tan, S. Mhaisalkar, X. Lu, Stress-induced structural changes in electrospun polyvinylidene difluoride nanofibers collected using a modified rotating disk, Polymer 49 (19) (2008) 4196–4203.
[23] Y.-S. Lee, G. Collins, T.L. Arinzeh, Neurite extension of primary neurons on electrospun piezoelectric scaffolds, Acta Biomaterialia 7 (11) (2011) 3877–3886.
[24] E. Bolbasov, K.S. Stankevich, E. Sudarev, V. Bouznik, V. Kudryavtseva, L. Antonova, V. Matveeva, Y.G. Anissimov, S. Tverdokhlebov, The investigation of the production method influence on the structure and properties of the ferroelectric nonwoven materials based on vinylidene fluoride–tetrafluoroethylene copolymer, Mater. Chem. Phys. 182 (2016) 338–346.
[25] S.-H. Park, H.B. Lee, S.M. Yeon, J. Park, N.K. Lee, Flexible and stretchable piezoelectric sensor with thickness-tunable configuration of electrospun nanofiber mat and elastomeric substrates, ACS Appl. Mater. Interfaces 8 (37) (2016) 24773–24781.

[26] G. Zandesh, A. Gheibi, M. Sorayani Bafqi, R. Bagherzadeh, M. Ghoorchian, M. Latifi, Piezoelectric electrospun nanofibrous energy harvesting devices: Influence of the electrodes position and finite variation of dimensions, J. Industr. Textiles 47 (3) (2017) 348–362.

[27] S.M. Damaraju, Y. Shen, E. Elele, B. Khusid, A. Eshghinejad, J. Li, M. Jaffe, T. L. Arinzeh, Three-dimensional piezoelectric fibrous scaffolds selectively promote mesenchymal stem cell differentiation, Biomaterials 149 (2017) 51–62.

[28] F. He, M. Sarkar, S. Lau, J. Fan, L.H. Chan, Preparation and characterization of porous poly (vinylidene fluoride-trifluoroethylene) copolymer membranes via electrospinning and further hot pressing, Polym. Test. 30 (4) (2011) 436–441.

[29] M. Baniasadi, Z. Xu, S. Moreno, S. Daryadel, J. Cai, M. Naraghi, M. Minary-Jolandan, Effect of thermomechanical post-processing on chain orientation and crystallinity of electrospun P(VDF-TrFE) nanofibers, Polymer 118 (2017) 223–235.

[30] P. Hitscherich, S. Wu, R. Gordan, L.H. Xie, T. Arinzeh, E.J. Lee, The effect of PVDF-TrFE scaffolds on stem cell derived cardiovascular cells, Biotechnol. Bioeng. 113 (7) (2016) 1577–1585.

[31] V. Sencadas, C. Ribeiro, J. Nunes-Pereira, V. Correia, S. Lanceros-Méndez, Fiber average size and distribution dependence on the electrospinning parameters of poly (vinylidene fluoride–trifluoroethylene) membranes for biomedical applications, Appl. Phys. A 109 (3) (2012) 685–691.

[32] Y.Y. Zhao, X. Li, C. Wang, L.J. Li, The effects of organic solvent on the electrospinning of water-soluble polyacrylamide with ultrahigh molecular weight, Solid State Phenomena, Trans Tech Publ (2007) 113–116.

[33] A. Haider, S. Haider, I.K. Kang, A comprehensive review summarizing the effect of electrospinning parameters and potential applications of nanofibers in biomedical and biotechnology, Arab. J. Chem. 11 (8) (2015) 1165–1188.

[34] K.J. Kim, G.B. Kim, Curie transition, ferroelectric crystal structure and ferroelectricity of a VDF/TrFE (7525) copolymer: 2. The effect of poling on Curie transition and ferroelectric crystal structure, Polymer 38 (19) (1997) 4881–4889.

[35] K.J. Kim, N.M. Reynolds, S.L. Hsu, Spectroscopic analysis of the crystalline and amorphous phases in a vinylidene fluoride/trifluoroethylene copolymer, Macromolecules 22 (12) (1989) 4395–4401.

[36] N. Weber, Y.S. Lee, S. Shanmugasundaram, M. Jaffe, T.L. Arinzeh, *Characterization and in vitro cytocompatibility of piezoelectric electrospun scaffolds*, Acta Biomater. 6 (9) (2010) 3550–3556.

[37] K. Tashiro, Y. Itoh, M. Kobayashi, H. Tadokoro, Polarized Raman spectra and LO-TO splitting of poly (vinylidene fluoride) crystal form I, Macromolecules 18 (12) (1985) 2600–2606.

[38] L. Trombi, S. Danti, S. Savelli, S. Moscato, D. D'Alessandro, C. Ricci, S. Giannotti, M. Petrini, Mesenchymal stromal cell culture and delivery in autologous conditions: a smart approach for orthopedic applications, J. Vis. Exp. 118 (2016) e5484.

[39] K.J. Livak, T.D. Schmittgen, Analysis of relative gene expression data using real-time quantitative PCR and the 2(-Delta Delta C(T)) method, Methods 4 (2001) 402–408.

[40] M. Bachmann, J. Koenig, Vibrational analysis of phase III of poly (vinylidene fluoride), J. Chem. Phys. 74 (10) (1981) 5896–5910.

[41] I.M. Ward, J. Sweeney. Mechanical properties of solid polymers, John Wiley & Sons, 2012.

[42] D. Li, J. Zhou, F. Chowdhury, J. Cheng, N. Wang, F. Wang, Role of mechanical factors in fate decisions of stem cells, Regen. Med. 6 (2) (2011) 229–240.

[43] L. Ghasemi-Mobarakeh, M.P. Prabhakaran, L. Tian, E. Shamirzaei-Jeshvaghani, L. Dehghani, S. Ramakrishna, Structural properties of scaffolds: crucial parameters towards stem cells differentiation, World Journal of Stem Cells 7 (4) (2015) 728.

[44] L. Krishna, K. Dhamodaran, C. Jayadev, K. Chatterjee, R. Shetty, S. Khora, D. Das, Nanostructured scaffold as a determinant of stem cell fate, Stem Cell Res Ther 7 (1) (2016) 188.

[45] T. Winkler, F. Sass, G. Duda, K. Schmidt-Bleek, A review of biomaterials in bone defect healing, remaining shortcomings and future opportunities for bone tissue engineering: The unsolved challenge, Bone Joint Res. 7 (3) (2018) 232–243.

[46] C. Ribeiro, J. Pärssinen, V. Sencadas, V. Correia, S. Miettinen, V.P. Hytönen, S. Lanceros-Méndez, Dynamic piezoelectric stimulation enhances osteogenic differentiation of human adipose stem cells, J. Biomed. Mater. Res. Part A 103 (6) (2015) 2172–2175.

[47] R. Sobreiro-Almeida, M. Tamaño-Machiavello, E. Carvalho, L. Cordón, S. Doria, L. Senent, D. Correia, C. Ribeiro, S. Lanceros-Méndez, R. Sabater i Serra, Human mesenchymal stem cells growth and osteogenic differentiation on piezoelectric poly (vinylidene fluoride) microsphere substrates, Int. J. Mol. Sci. 18 (11) (2017) 2391.

[48] L. Persano, C. Dagdeviren, Y. Su, Y. Zhang, S. Girardo, D. Pisignano, Y. Huang, J. A. Rogers, High performance piezoelectric devices based on aligned arrays of nanofibers of poly(vinylidenefluoride-co-trifluoroethylene), Nat. Commun. 4 (2013) 1633.

[49] S. Lyu, C. Huang, H. Yang, X. Zhang, Electrospun fibers as a scaffolding platform for bone tissue repair, J. Orthop. Res. 31 (9) (2013) 1382–1389.

[50] A. Matsugaki, Y. Isobe, T. Saku, T. Nakano, Quantitative regulation of bone-mimetic, oriented collagen/apatite matrix structure depends on the degree of osteoblast alignment on oriented collagen substrates, J. Biomed. Mater. Res. A 103 (2) (2015) 489–499.

[51] Y.S. Lee, G. Collins, Treena Livingston Arinzeh, Neurite extension of primary neurons on electrospun piezoelectric scaffolds, Acta Biomater. 7 (2011) 3877–3886.

[52] M.F. Leong, K.S. Chian, P.S. Mhaisalkar, W.F. Ong, B.D. Ratner, Effect of electrospun poly(D, L-lactide) fibrous scaffold with nanoporous surface on attachment of porcine esophageal epithelial cells and protein adsorption, Biomed. Mater. Res. 89A (2009) 1040–1048.

[53] Solvent comparison tool (Eastman) http://ws.eastman.com/Wizards/Esolvents/ESolvProperty.asp?Solvent=-1&property=288&printer=true.

[54] T. Uyar, F. Besenbacher, Electrospinning of uniform polystyrene fibers: The effect of solvent conductivity, Polymer 49 (24) (2008) 5336–5343.

[55] Q.P. Pham, U. Sharma, A.G. Mikos, Electrospinning of polymeric nanofibers for tissue engineering applications: a review, Tissue Eng 12 (5) (2006) 1197–1211.

[56] H. Yi, F. Ur Rehman, C. Zhao, B. Liu, N. He, Recent advances in nano scaffolds for bone repair, Bone Res. 4 (2016) 16050.

[57] A. Baji, Y.-W. Mai, S.-C. Wong, M. Abtahi, P. Chen, Electrospinning of polymer nanofibers: effects on oriented morphology, structures and tensile properties, Compos. Sci. Technol. 70 (5) (2010) 703–718.

[58] K. Rezwana, Q.Z. Chen, J.J. Blakera, A.R. Boccaccinia, Biodegradable and bioactive porous polymer/inorganic composite scaffolds for bone tissue engineering, Biomaterials 27 (18) (2006) 3413–34361.

[59] W.A. Yee, M. Kotaki, Y. Liu, Lu. Xuehong, Morphology, polymorphism behavior and molecular orientation of electrospun poly (vinylidene fluoride) fibers, Polymer 48 (2) (2007) 512–521.

[60] B. Azimi, P. Nourpanah, M. Rabiee, S. Arbab, M. Grazia Cascone, A. Baldassare, L. Lazzeri, Application of the dry-spinning method to produce poly (ε-caprolactone) fibers containing bovine serum albumin laden gelatin nanoparticles, J. Appl. Polym. Sci. 133 (48) (2016).

[61] F. Mokhtari, M. Shamshirsaz, M. Latifi, S. Asadi, Comparative evaluation of piezoelectric response of electrospun PVDF (polyvinilydine fluoride) nanofiber with various additives for energy scavenging application, J. Textile Institute 108 (6) (2017) 906–914.

[62] P. Kumar, R. Vasita, Understanding the relation between structural and mechanical properties of electrospun fiber mesh through uniaxial tensile testing, J. Appl. Polym. Sci. 134 (26) (2017) 45012.

[63] H.M. Pauly, D.J. Kelly, K.C. Popat, N.A. Trujillo, N.J. Dunne, H.O. McCarthy, T. L. Haut Donahue, Mechanical properties and cellular response of novel electrospun nanofibers for ligament tissue engineering: effects of orientation and geometry, J. Mech. Behav. Biomed. Mater. 61 (2016) 258–270.

[64] S. Ma, T. Ye, T. Zhang, Z. Wang, K. Li, M. Chen, J. Zhang, Z. Wang, S. Ramakrishna, L. Wei, Highly oriented electrospun P(VDF-TrFE) fibers via mechanical stretching for wearable motion sensing, Adv. Mater. Technol. (2018) 1800033.

[65] A. Wang, M. Hu, L. Zhou, X. Qiang, Self-Powered well-aligned P(VDF-TrFE) piezoelectric nanofiber nanogenerator for modulating an exact electrical stimulation and enhancing the proliferation of preosteoblasts, Nanomaterials 9 (2019) 349.

[66] V. Karageorgiou, D. Kaplan, Porosity of 3D biomaterial scaffolds and osteogenesis, Biomaterials 26 (27) (2005) 5474–5491.

[67] C. Ricci, L. Trombi, I. Soriga, F. Piredda, M. Milazzo, C. Stefanini, L. Bruschini, G. Perale, G. Pertici, S. Danti, Investigating the microenvironmental effects of scaffold chemistry and topology in human mesenchymal stromal cell/polymeric hollow microfiber constructs, Biomed. Sci. Eng. 2 (2016) 8–17.

[68] S. Danti, G. Ciofani, S. Moscato, D. D'Alessandro, E. Ciabatti, C. Nesti, R. Brescia, G. Bertoni, A. Pietrabissa, M. Lisanti, M. Petrini, V. Mattoli, S. Berrettini, Boron nitride nanotubes and primary human osteoblasts: In vitro compatibility and biological interactions under low frequency ultrasound stimulation, Nanotechnology 24 (46) (2013) 465102.

[69] G. Strangis, M. Labardi, G. Gallone, M. Milazzo, S. Capaccioli, F. Forli, P. Cinelli, S. Berrettini, M. Seggiani, S. Danti, P. Parchi, 3D Printed Piezoelectric $BaTiO_3$/Polyhydroxybutyrate Nanocomposite Scaffolds for Bone Tissue Engineering, Bioengineering 11 (2024) 193.

[70] D. D'Alessandro, C. Ricci, M. Milazzo, G. Strangis, F. Forli, G. Buda, M. Petrini, S. Berrettini, M.J. Uddin, S. Danti, P. Parchi, Piezoelectric Signals in Vascularized Bone Regeneration, Biomolecules 11 (2021) 1731.

[71] G. Ciofani, S. Danti, L. Ricotti, D. D'Alessandro, S. Moscato, S. Berrettini, V. Mattoli, A. Menciassi, Boron nitride nanotubes: Production, properties, biological interactions and potential applications as therapeutic agents in brain diseases, Curr. Nanosci. 7 (1) (2011) 94–109.